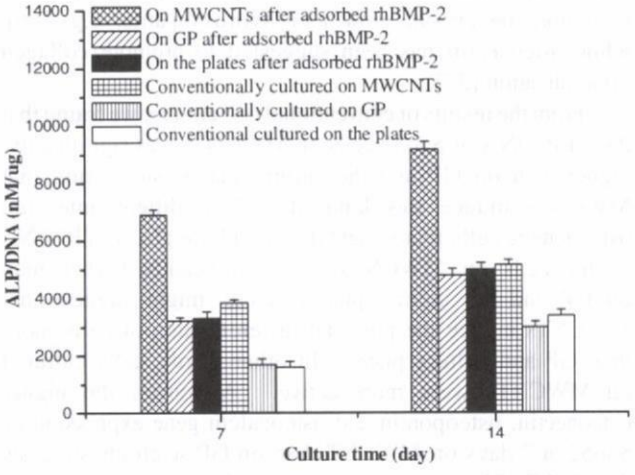

Figure 6. ALP/DNA of the SaoS2 cells cultured on samples with and without the adsorption of rhBMP-2 in advance ($n = 4$).

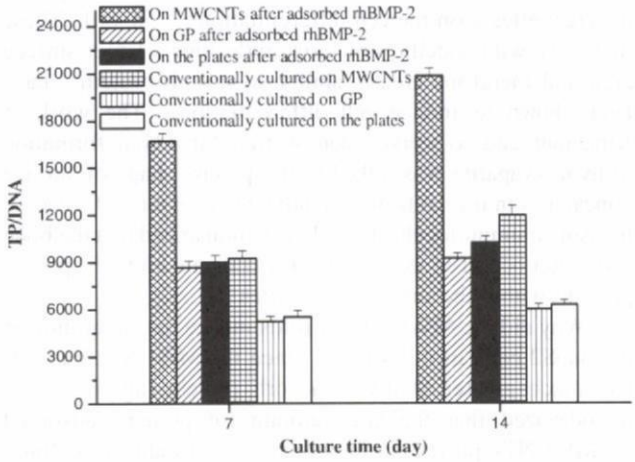

Figure 7. Total-protein/DNA of the SaoS2 cells cultured on samples with and without the adsorption of rhBMP-2 in advance ($n = 4$).

osteopontin and osteocalcin gene expression of SaoS2 at day 14 between GP and control ($P > 0.05$).

Figure 6 shows ALP/DNA of the SaoS2 cells on the samples after adsorbing rhBMP-2 at day 7 and day 14, compared with the results of the conventional cell culture. ALP/DNA of the cells on all the samples increased after the adsorption of rhBMP-2. But the value for MWCNTs increased most significantly. The value for GP and the control had no significant difference even after the adsorption of rhBMP-2 ($P > 0.05$).

TP/DNA of the SaoS2 cells on the samples after adsorbing rhBMP-2 at day 7 and day 14, compared with the results of the conventional cell culture, is shown in figure 7. The TP/DNA of cells on all the samples all increased after the adsorption of rhBMP-2. But the value for MWCNTs increased most observably. The value for GP and the culture plates had no significant difference even after the adsorption of rhBMP-2 ($P > 0.05$).

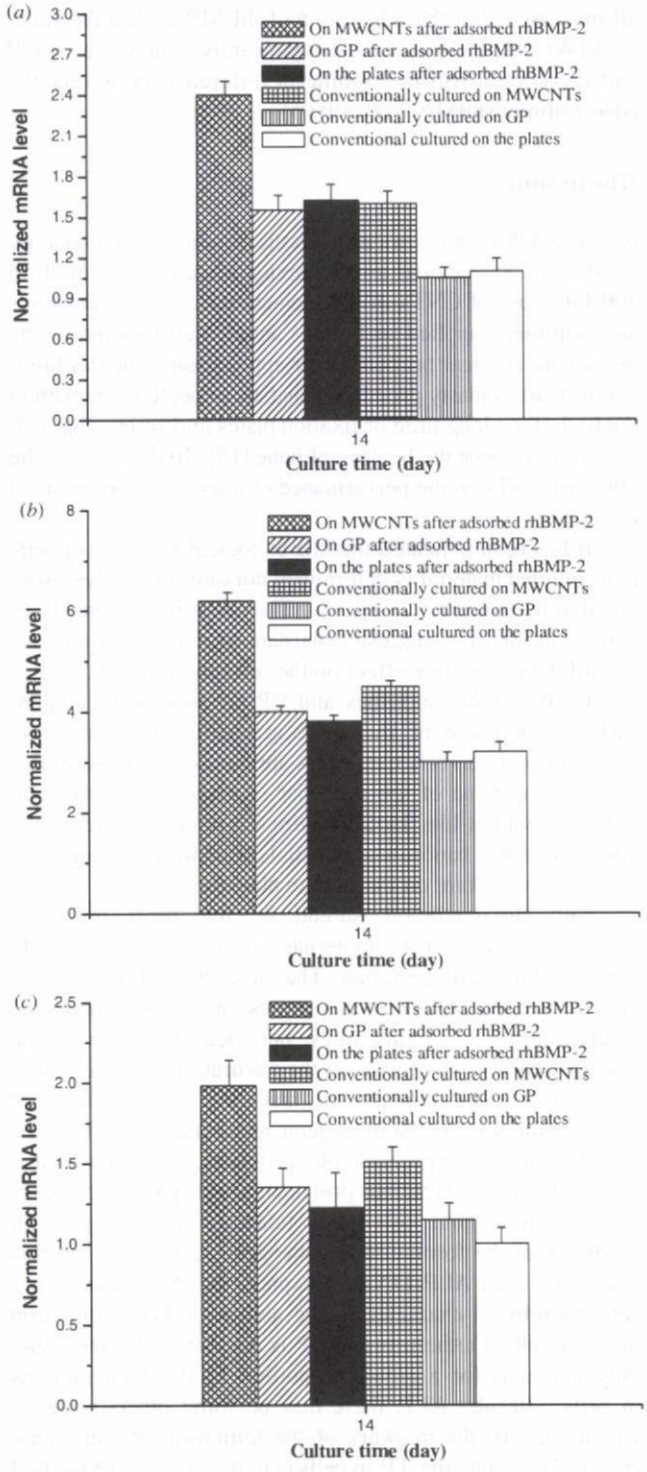

Figure 8. Gene expression of (*a*) osteonectin, (*b*) osteocalcin and (*c*) osteopontin normalized by the gene expression of 18S of cells cultured on the different samples with and without the adsorption of rhBMP-2 in advance ($n = 4$).

Figure 8 shows osteonectin, osteopontin and osteocalcin gene expression of the SaoS2 cells on the samples after adsorbing rhBMP-2 at day 14, compared with the results of the conventional cell culture. Osteonectin, osteopontin and

osteocalcin gene expression of the cells on all the samples all increased after the adsorption of rhBMP-2. But the value for MWCNTs increased most significantly. The value for GP and the control had no significant difference even after the adsorption of rhBMP-2 ($P > 0.05$).

Discussion

Because CNTs have a high elastic modulus, approaching 1 TPa, and exceptional tensile strengths, ranging from 20 to 100 GPa, use of CNTs in the biomaterials, such as ceramics and polymers, applied to bone is anticipated to improve the overall mechanical properties for applications, such as high-strength arthroplasty prostheses that are expected to remain in the body for a long time or fixation plates and screws that will not fail or impede the healing of bone [15]. In these cases, the effect of CNTs on the performance of osteoblasts seems most important.

It has been indicated that the biological response of cells to implanted material is determined not only by its chemistry, but also by structure [2, 47, 48]. The nano-dimensionality of nature has logically suggested that nanostructured biomaterials should have a positive effect on the cell functions [49, 50].

Both carbon nanotubes and GP are isomorphs of pure carbon, composed of the same grapheme sheet structure. However, only carbon nanotubes are nano-scaled. So in this study, comparison of the influence of carbon nanotubes and GP on osteoblast-like SaoS2 *in vitro* was done to figure out the effect of carbon nanotubes on cellular functions. Meanwhile, we used cell culture on the culture plate as a control.

Cell differentiation should be the most important evaluation point for biomaterials because it may directly contribute to the tissue repair. The satisfactory differentiation and maturation of osteoblasts are essential for bone tissue regeneration. So in this study, our focus has been on the effect of carbon nanotubes on the maturation of the cultured osteoblasts. This may be the first time that the effect of carbon nanotubes on the osteogenic maturation, especially the osteoblastic gene expression of osteoblasts, was researched.

ALP, a noncollagenous protein, is a highly specific marker of bone formation, osteoblast function and a significant predictor of the formation of osteogenic cells [51]. In this study, we used ALP/DNA to express the ALP activity per cell, thereby to characterize the ability of bone formation of each cell. Furthermore, ALP is one kind of protein and only accounts for a small proportion of the total proteins in cells. Besides ALP, there may be some others proteins, which may be the markers of the formation of osteogenic cells [52]. Evaluating TP in cells may be an effective method for evaluating the potential differentiation of cells. So, in our study, TP/DNA was used as an additional marker of the activity per unit cell for the potential cell differentiation.

Osteocalcin, osteopontin and osteonectin are important osteoblastic markers and are expressed at different maturation stages of the osteoblasts [53]. These three genes have been shown to be differently involved in the bone mineralization process. Osteocalcin, which is the most osteoblast-specific gene yet known [54], has been demonstrated to stimulate bone mineral maturation [55]. Osteopontin has been shown to inhibit the crystal growth of hydroxyapatite, e.g. [56], while osteonectin has been suggested to promote collagen mineralization [57].

From the results of conventional cell culture, we found that the ALP/DNA of SaoS2 cells on MWCNTs was significantly higher than on GP and the culture plates, suggesting that MWCNTs induce this kind of cell to differentiate into osteogenetic cells more than GP and culture plates. TP/DNA of the cells on MWCNTs was significantly higher than on GP and the culture plates, which might suggest that MWCNTs induce the potential differentiation of cells more than GP and culture plates. In other words, cells cultured on MWCNTs were more active. Moreover, the higher osteonectin, osteopontin and osteocalcin gene expression of SaoS2 at 7 days on MWCNT than on GP scaffolds suggests that the MWCNT scaffolds could provide a better environment for the mineralization process and the osteoblastic maturation.

Some publications have shown that, although some materials had the same chemical composition, they had different effects on the cell differentiation [2, 58–60]. These materials, with specific structures, indicating a larger surface area and therefore greater ability to adsorb proteins, have been shown to induce cell differentiation. The work of Ripamonti and co-workers demonstrated that bone formation in hydroxyapatite was linked to the precise shape of surface concavities in implants, which indicated a larger surface area; by using immunolocalization, they demonstrated that the bone formation occurred as a result of a concentration of specific proteins within the surface concavities [61, 62].

Why did the MWCNT scaffolds induce the maturation of the SaoS2 cells in this study? Since the MWCNT scaffolds had much greater ability to adsorb protein (figure 2), we hypothesized that the large amount of proteins adsorbed on MWCNTs played an important role in inducing cellular functions.

To confirm this hypothesis, we immersed the samples in the culture medium containing rhBMP-2 to make them adsorb more proteins before cell culture. The results showed that after the adsorption of rhBMP-2, both TP/DNA and ALP/DNA increased on all samples. Impressively, the value for MWCNTs increased most significantly. The increments of TP/DNA and ALP/DNA for MWCNTs were respectively about 11 times and 18 times those for GP and the control at both day 4 and day 7. Therefore, the results of cell culture after the adsorption of rhBMP-2 might be an effective proof for our hypothesis.

Hing [63] has reported that competitive protein adsorption at a bioactive surface may vary in three ways, which is the quantity of protein adsorbed, the species of protein adsorbed and the confirmation of the adsorbed protein. Also, he supposed that nanostructures might thus influence protein adsorption by providing a larger surface area, thereby increasing the quantity of adsorbed growth factors above a critical level for cell recruitment and activation. In our study, we substantiated the importance of the protein adsorption. Carbon nanotubes might adsorb a large number of proteins due to their larger surface area and unique electronic, catalytic

and chemical properties. These proteins might be helpful for the cell differentiation and maturation of the osteoblasts and therefore directly contribute to bone tissue repair. Since *in vivo* cellular microenvironments are immobilized within tissue, and consist of diverse extracellular matrix proteins, CNTs might induce cellular functions *in vivo* by adsorbing a large number of proteins.

Conclusion

Carbon nanotubes might induce the osteoblastic differentiation and osteogenic maturation of the cultured human osteoblast-like cells (SaoS2) by adsorbing a large number of proteins, which indicated that carbon nanotubes might be a candidate scaffold material for bone tissue engineering.

Acknowledgment

This study was financially supported by JSPS (Japan Society for the Promotion of Science).

References

[1] Li X M, Feng Q L, Liu X H, Dong W and Cui F Z 2006 Collagen-based implants reinforced by chitin fibres in a goat shank bone defect model *Biomaterials* **27** 1917–23

[2] Li X M, Van Blitterswijk C A, Feng Q L, Cui F Z and Watari F 2008 The effect of calcium phosphate microstructure on bone-related cells *in vitro Biomaterials* **29** 3306–16

[3] Capito R M and Spector M 2007 Collagen scaffolds for nonviral IGF-1 gene delivery in articular cartilage tissue engineering *Gene Therapy* **14** 721–32

[4] Spector M 2006 Biomaterials-based tissue engineering and regenerative medicine solutions to musculoskeletal problems *Swiss Med. Wkly* **136** 293–301

[5] Li X M, Feng Q L, Wang W J and Cui F Z 2006 Chemical characteristics and cytocompatibility of collagen-based scaffold reinforced by chitin fibers for bone tissue engineering *J. Biomed. Mater. Res.* **77B** 219–26

[6] Li X M, Gao H, Uo M, Sato Y, Akasaka T, Feng Q L, Cui F Z, Liu X H and Watari F 2008 Effect of carbon nanotubes on cellular functions in vitro *J. Biomed. Mater. Res.* A (DOI: 10.1002/jbm.a.32203)

[7] Li X M, Feng Q L, Jiao Y F and Cui F Z 2005 Collagen-based scaffolds reinforced by chitosan fibres for bone tissue engineering *Polym. Int.* **54** 1034–40

[8] Venugopal J, Low S, Choon A T and Ramakrishna S 2008 Interaction of cells and nanofiber scaffolds in tissue engineering *J. Biomed. Mater. Res.* **84B** 34–48

[9] Labhasetwar V 2005 What is next for nanotechnology? *J. Biomed. Nanotechnol.* **1** 373–4

[10] Webster T J, Hellenmeyer E L and Price R L 2005 Increased osteoblast functions on theta plus delta nanofiber alumina *Biomaterials* **26** 953–60

[11] Watari F *et al* 2008 Behavior of *in vitro*, *in vivo* and internal motion of micro/nano particles of titanium, titanium oxides and others *J. Ceram. Soc. Japan* **116** 1–5

[12] Watari F, Yokoyama A, Omori M, Hirai T, Kondo H, Uo M and Kawasaki T 2004 Biocompatibility of materials and development to functionally graded implant for bio-medical application *Compos. Sci. Technol.* **64** 893–908

[13] Yokoyama A *et al* 2005 Biological behavior of hat-stacked carbon nanofibers in the subcutaneous tissue in rats *Nano. Lett.* **5** 157–61

[14] Harrison B S and Atala A 2007 Carbon nanotube applications for tissue engineering *Biomaterials* **28** 344–53

[15] Usui Y *et al* 2008 Carbon nanotubes with high bone-tissue compatibility and bone-formation acceleration effects *Small* **4** 240–6

[16] Firkowska I, Olek M, Pazos-Perez N, Rojas-Chapana J and Giersig M 2006 Highly ordered MWNT-based matrixes: topography at the nanoscale conceived for tissue engineering *Langmuir* **22** 5427–34

[17] Aoki N, Yokoyama A, Nodasaka Y, Akasaka T, Uo M, Sato Y, Tohji K and Watari F 2006 Strikingly extended morphology of cells grown on carbon nanotubes *Chem. Lett.* **35** 508–9

[18] Correa-Duarte M A, Wagner N, Rojas-Chapana J, Morsczeck C, Thie M and Giersig M 2004 Fabrication and biocompatibility of carbon nanotube-based 3D networks as scaffolds for cell seeding and growth *Nano Lett.* **4** 2233–6

[19] Uo M, Tamura K, Sato Y, Yokoyama A, Watari F, Totsuka Y and Tohji K 2005 The cytotoxicity of metal-encapsulating carbon nanocapsules *Small* **1** 816–9

[20] Akasaka T and Watari F 2005 Nano-architecture on carbon nanotube surface by biomimetic coating *Chem. Lett.* **34** 826–7

[21] MacDonald R A, Laurenzi B F, Viswanathan G, Ajayan P M and Stegeman J P 2005 Collagen-carbon nanotube composite materials as scaffolds in tissue engineering *J. Biomed. Mater. Res.* **74A** 489–96

[22] Kam N W S, Jessop T C, Wender P A and Dai H 2004 Nanotube molecular transporters: internalization of carbon nanotube–protein conjugates into mammalian cells *J. Am. Chem. Soc.* **126** 6850–1

[23] Kam N W S, Liu Z and Dai H 2005 Functionalization of carbon nanotubes via cleavable disulfide bonds for efficient intracellular delivery of siRNA and potent gene silencing *J. Am. Chem. Soc.* **127** 12492–3

[24] Supronowicz P R, Ajayan P M, Ullmann K R, Arulanandam B P, Metzger D W and Bizios R 2002 Novel current-conducting composite substrates for exposing osteoblasts to alternating current stimulation *J. Biomed. Mater. Res.* **59** 499–506

[25] Chen R L, Bangsaruntip S, Drouvalakis K A, Kam N W S, Shim M and Li Y 2003 Noncovalent functionalization of carbon nanotubes for highly specific electronic biosensors *Proc. Natl Acad. Sci.* **100** 4984–9

[26] Kiura K, Sato Y, Yasuda M, Fugetsu B, Watari F, Tohji K and Shibata K 2005 Activation of human monocytes and mouse splenocytes by single-walled carbon nanotubes *J. Biomed. Nanotechnol.* **1** 359–64

[27] Sato Y *et al* 2005 Influence of length on cytotoxicity of multi-walled carbon nanotubes against human acute monocytic leukemia cell line THP-I *in vitro* and subcutaneous tissue of rats *in vivo Mol. Biosyst.* **1** 176–82

[28] Pantarotto D, Briand J, Prato M and Pianco A 2004 Translocation of bioactive peptides across cell membranes by carbon nanotubes *Chem. Commun.* **10** 16–7

[29] Mwenifumbo S, Shaffer M S and Stevens M M 2007 Exploring cellular behaviour with multi-walled carbon nanotube constructs *J. Mater. Chem.* **17** 1894–902

[30] Lu Q, Moore J M, Huang G, Mount A S, Rao A M and Larcom L L 2004 RNA polymer translocation with single-walled carbon nanotubes *Nano Lett.* **4** 2473–77

[31] Cherukuri P, Bachilo S M, Litovsky S H and Weisman R B 2004 Near-infrared fluorescence microscopy of single-walled carbon nanotubes in phagocytic cells *J. Am. Chem. Soc.* **126** 15638–9

[32] Bianco A, Hoebeke J, Godefroy S, Chaioin O, Pantarotto D and Briand J P 2005 Cationic carbon nanotubes bind to CpG oligodeoxynucleotides and enhance their immunostimulatory properties *J. Am. Chem. Soc.* **127** 58–9

[33] Zanello L P, Zhao B, Hu H and Haddon R C 2006 Bone cell proliferation on carbon nanotubes *Nano Lett.* **6** 562–7
[34] Hu H, Ni Y, Montana V, Haddon R C and Parpura V 2004 Chemically functionalized carbon nanotubes as substrates for neuronal growth *Nano Lett.* **4** 507–11
[35] Chen X, Tam U C, Czlapinski J L, Lee G S, Rabuka D and Zettl A 2006 Interfacing carbon nanotubes with living cells *J. Am. Chem. Soc.* **128** 6292–3
[36] Hu H, Ni Y, Mandal S K, Montana V, Zhao B and Haddon R C 2005 Polyethyleneimine functionalized single-walled carbon nanotubes as a substrate for neuronal growth *J. Phys. Chem.* B **109** 4285–9
[37] Kakudo N, Shimotsuma A, Miyake S, Kushida S and Kusumoto K 2008 Bone tissue engineering using human adipose-derived stem cells and honeycomb collagen scaffold *J. Biomed. Mater. Res.* **84A** 191–7
[38] Li H Y, Zhai W Y and Chang J 2008 *In vitro* biocompatibility assessment of PHBV/Wollastonite composites *J. Mater. Sci. Mater. Med.* **19** 67–73
[39] Bai H and Wang Z Z 2008 Directing human embryonic stem cells to generate vascular progenitor cells *Gene Therapy* **15** 89–95
[40] Gosain A K, Riordan P A, Song L S, Amarante M T, Kalantarian B, Nagy P G, Wilson C R, Toth J M and McIntyre B L 2004 A 1-year study of osteoinduction in hydroxyapatite-derived biomaterials in an adult sheep model: II. Bioengineering implants to optimize bone replacement in reconstruction of cranial defects *Plast. Reconstr. Surg.* **114** 1155–63
[41] Park J W, Suh J Y and Chung H J 2008 Effects of calcium ion incorporation on osteoblast gene expression in MC3T3-E1 cells cultured on microstructured titanium surfaces *J. Biomed. Mater. Res.* **86A** 117–26
[42] Li X M, Feng Q L and Cui F Z 2006 *In vitro* degradation of porous nano-hydroxyapatite/collagen/PLLA scaffold reinforced by chitin fibres *Mater. Sci. Eng.* C **26** 716–20
[43] Fujibayashi S, Neo M, Kim H M, Kokubo T and Nakamura T 2004 Osteoinduction of porous bioactive titanium metal *Biomaterials* **25** 443–50
[44] Popat K C, Chatvanichkul K I, Barnes G L, Latempa T J, Grimes C A and Desai T A 2007 Osteogenic differentiation of marrow stromal cells cultured on nanoporous alumina surfaces *J. Biomed. Mater. Res.* **80A** 955–64
[45] Yim E K F, Pang S W and Leong K W 2007 Synthetic nanostructures inducing differentiation of human mesenchymal stem cells into neuronal lineage *Exp. Cell Res.* **313** 1820–9
[46] Ou K L, Lin C T, Chen S L, Huang C F, Cheng H C, Yeh Y M and Lin K H 2008 Effect of multi-nano-titania film on proliferation and differentiation of mouse fibroblast cell on titanium *J. Electrochem. Soc.* **155** E79–84
[47] Ratner B D, Johnston A B and Lenk T S 1987 Biomaterials surfaces *J. Biomed. Mater. Res.* **21(A1)** 59–90
[48] Zreiqat H, Standard O C, Gengenbach T, Steele J and Howlett C R 1996 The role of surface characteristics in the initial adhesion of human bone-derived cells on ceramics *Cell Mater.* **6** 45–6
[49] Abrams G A, Goodman S L, Nealey P F, Franco M and Murphy C J 2000 Nanoscale topography of the basement membrane underlying the corneal epithelium of the rhesus macaque *Cell Tissue Res.* **299** 39–46
[50] Kumazawa R, Watari F, Takashi N, Tanimura Y, Uo M and Totsuka Y 2002 Effects of Ti ions and particles on neutrophil function and morphology *Biomaterials* **23** 3757–64
[51] Havill L M, Rogers J, Cox L A and Mahaney M C 2006 QTL with pleiotropic effects on serum levels of bone-specific alkaline phosphatase and osteocalcin maps to the baboon ortholog of human chromosome 6p23–21.3 *J. Bone Miner. Res.* **21** 1888–96
[52] Smink J J, Begay V and Leutz A 2005 CCAAT/enhancer binding protein (C/EBP) beta is involved in bone formation *Bone* **36** S269
[53] Lian J B and Stein G S 1996 *Osteoblast Biology* ed R Marcus, D Feldman and J Kelsey (San Diego: Academic)
[54] Ducy P and Karsenty G 1998 Genetic control of cell differentiation in the skeleton *Curr. Opin. Cell Biol.* **10** 614–9
[55] Boskey A L, Gadaleta S, Gundberg C, Doty S B, Ducy P and Karsenty G 1998 Fourier transform infrared microspectroscopic analysis of bones of osteocalcin-deficient mice provides insight into the function of osteocalcin *Bone* **23** 187–96
[56] Ayukawa Y, Takeshita F, Inoue T, Yoshinari M, Shimono M, Suetsugu T and Tanaka T 1998 An immunoelectron microscopic localization of noncollagenous bone proteins (osteocalcin and osteopontin) at the bone-titanium interface of rat tibiae *J. Biomed. Mater. Res.* **41** 111–9
[57] Termine J D, Kleinman H K, Whitson S W, Conn K M, McGarvey M L and Martin G R 1981 Osteonectin, a bone-specific protein linking mineral to collagen *Cell* **26** 99–105
[58] Kilpadi K L, Sawyer A A, Prince C W, Chang P L and Bellis S L 2003 Primary human marrow stromal cells and SaOs-2 osteosarcoma cells use different mechanisms to adhere to hydroxylapatite *J. Biomed. Mater. Res.* **68A** 273–85
[59] Kondo N *et al* 2006 Osteoinduction with highly purified beta-tricalcium phosphate in dog dorsal muscles and the proliferation of osteoclasts before heterotopic bone formation *Biomaterials* **27** 4419–27
[60] Yamasaki H and Sakai H 1992 Osteogenic response to porous hydroxyapatite ceramics under the skin of dogs *Biomaterials* **13** 308–12
[61] Ripamonti U, Van den Heever B and Van Wyk J 1993 Expression of the osteogenic phenotype in porous hydroxyapatite implanted extraskeletally in Baboons *Matrix* **13** 491–502
[62] Magan A and Ripamonti U 1996 Geometry of porous hydroxyapatite implants influences osteogenesis in baboons (*Papio Ursinus*) *J. Craniofac. Surg.* 7 71–8
[63] Hing K A 2005 Bioceramic bone graft substitutes: influence of porosity and chemistry *Int. J. Appl. Ceram. Technol.* **2** 184–99

IOP PUBLISHING JOURNAL OF PHYSICS D: APPLIED PHYSICS

J. Phys. D: Appl. Phys. **41** (2008) 024006 (6pp) doi:10.1088/0022-3727/41/2/024006

Damage-free surface treatment of carbon nanotubes and self-assembled monolayer devices using a neutral beam process for fusing top–down and bottom–up processes

Seiji Samukawa[1], Yasushi Ishikawa[1], Keiji Okumura[1], Yoshinori Sato[2], Kazuyuki Tohji[2] and Takao Ishida[3]

[1] Institute of Fluid Science, Tohoku University, Aoba-ku, Sendai, 980-8577, Japan
[2] Graduate School of Environmental Studies, Tohoku University, Aoba-ku, Sendai, 980-8579, Japan
[3] Nanotechnology Research Institute, National Institute of Advanced Industrial Science and Technology, Tsukuba, 305-8562, Japan

E-mail: samukawa@ifs.tohoku.ac.jp

Received 5 June 2007, in final form 15 August 2007
Published 4 January 2008
Online at stacks.iop.org/JPhysD/41/024006

Abstract

Plasma etching processes have been used for the past 30 years to shrink the pattern size of integrated devices. However, the inherent problems of plasma processes, such as ultraviolet photon radiation damage, limit the effectiveness of etching and surface treatments of nanoscale devices. To overcome these problems, we developed a neutral beam surface treatment process. The process uses neutral beams and a defect-free surface process to fabricate carbon nanotubes and self-assemble mono-layer devices. We found that neutral beams can be used to produce atomically defect-free surfaces in carbon nanotubes and organic molecules. This technique has potential for fabricating nanodevices.

(Some figures in this article are in colour only in the electronic version)

1. Introduction

Plasma processes have been widely used to shrink the pattern size of ultra-large-scale integrated (ULSI) devices. Recent ULSI production processes can fabricate sub-50 nm patterns on Si wafers. The use of high-density plasma sources, such as inductively coupled plasma (ICP) and electron-cyclotron-resonance (ECR) plasma, has been important for developing precise surface processes. However, these sources have problems, including radiation damage caused by charge buildup from positive ions and electrons [1–4] and by ultraviolet (UV), vacuum ultraviolet (VUV) and x-ray photons [5–12]. High-density crystal defects are generated and material structures are destroyed by UV or VUV photons radiating from the plasma to the etched surface [13]. These serious problems must be overcome if future nanoscale devices, such as molecular devices (organic molecular and DNA, etc) or single-walled carbon nanotube field effect transistors, are to be fabricated.

We think that bio-supermolecules (e.g. DNA and proteins), organic molecules (e.g. self-assembling monolayers (SAMs)), and single-walled carbon nanotubes (SWCNTs) will be used in active areas on silicon in future nanodevices. For these devices, it will be necessary to fuse top–down (surface modification, etching, doping and deposition) and bottom–up (ability of nanostructures to self-assemble by using SAMs and SWCNTs) processes to integrate these new materials on silicon substrates and to attain the desired electrical characteristics. However, new materials, such as SAMs, DNA, protein and SWCNTs, are very susceptible to damage caused by UV radiation from plasma.

We conducted a preliminary investigation of plasma radiation damage caused by N_2 and Ar plasma to new materials, such as SAMs and SWCNTs. Additionally, to find a

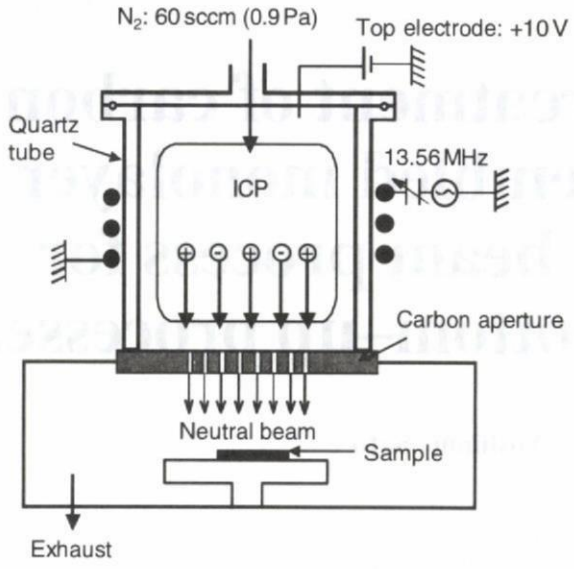

Figure 1. Our neutral beam generation system for surface treatment.

damage-free process, we investigated the possibility of using neutral beam processes to fabricate nanoscale devices.

2. Experimental

A schematic diagram of our neutral beam (NB) source is shown in figure 1. It consists of an ICP source and parallel carbon plates. The plasma chamber is separated from the process chamber by an array of carbon aperture plates. A more detailed diagram is presented elsewhere [14]. The carbon electrode has many apertures, each with an aspect ratio of about 10 (diameter: 1 mm, length: 10 mm). The aperture open area is 50% of an area 100 mm in diameter on the bottom carbon plate. Their purpose is to extract neutral beams from the plasma in the process chamber. High-density ICP was generated by applying a radio frequency power of 13.56 MHz. When the accelerated ions passed through the carbon apertures, they were neutralized through charge exchange with the aperture walls. As a result, an energetic neutral beam (with very few charged particles) irradiated the surface. The neutralization efficiency of the accelerated ions was more than 95% [15]. In addition, the carbon apertures minimized the UV photon irradiation on the substrate. They can reduce UV photon flux to less than a few per cent of that in a conventional plasma process (figure 2) [15].

We also investigated irradiation of N_2 and Ar gas plasma at a pressure of 0.9 Pa to treat the surfaces of SAMs and SWCNTs by setting the sample (substrate) on the bottom carbon aperture plate in the same neutral beam source. The estimated bombardment energies of neutral beams and ions from the plasma were about 10 eV [15]. Additionally, when we controlled the plasma generation power, the ion flux in N_2 and Ar ICP was the same (about 6×10^{15} cm^{-2} s^{-1}) as in the neutral beam flux.

Terphenyl methanethiol self-assembled monolayers (TP1-SAMs, figure 3) were formed on an atomically flat Au (1 1 1) surface. The deposition of atomically flat Au on mica has been described elsewhere [16]. The Au substrate was immersed in a

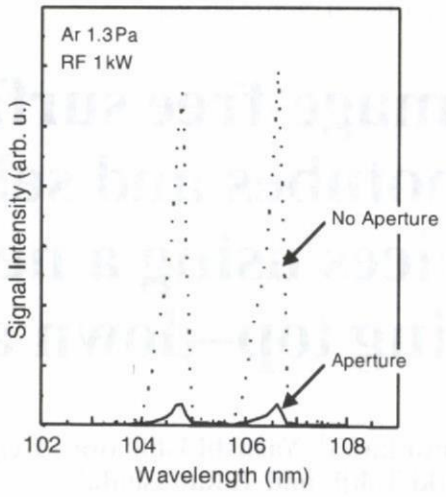

Figure 2. UV spectra and intensity obtained from Ar plasma and elimination of UV irradiation from Ar plasma to substrate using carbon apertures.

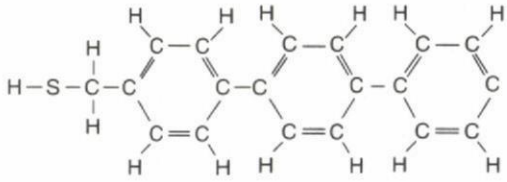

Figure 3. Schematic structure of terphenyl methanethiol self-assembled monolayer for plasma and neutral beam treatment.

0.1 mM TP1 CH_2Cl_2 solution for 24 h and then rinsed with pure CH_2Cl_2 solvent to remove any physisorbed multilayers that had formed. We used x-ray photoelectron spectroscopy (XPS) and time-of-flight secondary ion mass spectroscopy (TOF-SIMS) to analyse the chemical states of the surfaces. The XPS spectra were recorded with a SPECS (HAS 3500) spectrometer using an Mg Kα x-ray source at 200 W and 12 kV. The TOF-SIMS was measured with a Physical Electronics TFS-2000 using $^{69}Ga^+$ as the primary ion.

For the surface treatment of CNTs, we used single-walled carbon nanotubes (SWCNTs) that were synthesized with a direct current arc-discharge between a pure graphite cathode and a metal-loaded graphite anode in a helium atmosphere [17]. The cathode was a pure graphite rod (99.99% purity) with a diameter of 16 mm and a length of 50 mm, and the anode was a graphite rod (99.9% purity) with a diameter of 6 mm and a length of 85 mm. The anode was placed in a catalyst powder of Fe/Ni/C/S (= 1 : 1 : 3 : 0.1 weight ratio). The soot samples were synthesized using He gas (99.99%) at 100 Torr and an arc-discharge current of 70 A. The samples were collected only from the inner wall of the chamber. In the raw soot, SWCNTs coexist with many by-products such as metal particles, fullerenes and amorphous carbon. Therefore, they were separated from the impurities using the following purification process. First, fullerenes and amorphous carbon were burned out by heating approximately 600 mg of raw soot at 723 K and leaving it for 30 min in air. Then, the residual soot was heated to 773 K and left for 30 min in air to burn out the graphitic layers surrounding the metal particles. Finally,

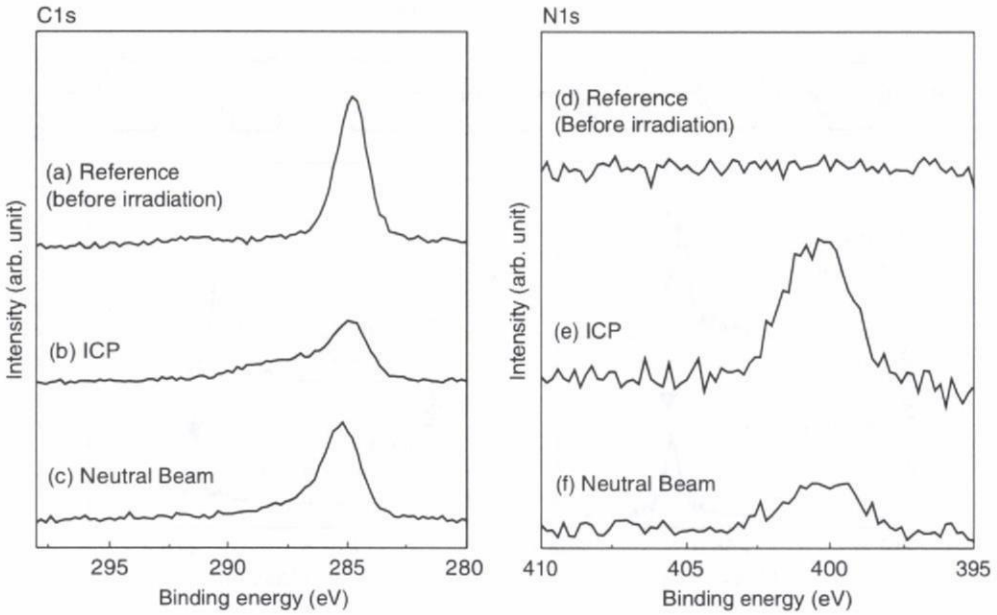

Figure 4. XPS spectra of TP1-SAMs before and after ICP and NB irradiation. (*a*) C(1s) region before irradiation, (*b*) C(1s) region after ICP process, (*c*) C(1s) region after NB process, (*d*) N(1s) region before irradiation, (*e*) N(1s) region after ICP process and (*f*) N(1s) region after NB process [18].

the metal particles were washed out of the soot by treating it with a 6 M hydrochloric acid solution. The processed soot was filtered and rinsed with deionized water.

We used a transmission electron microscope (TEM) (Hitachi HF-2000) with a field emission electron gun to observe the morphology of the soot and a Raman spectrometer (Jobin-Yvon T64000) to analyse the physical properties of the radial SWCNTs. We measured the samples in a backscattering configuration by using a laser with an excitation wavelength of 488.0 nm. The Raman scattering peaks corresponding to 1590 cm^{-1} in the tangential mode range were due to the zone folding effect of the SWCNTs. Since the peak at 1350 cm^{-1} is the Raman active mode of the defective carbon network, the intensity is roughly proportional to the amount of amorphous carbon in the sample. Therefore, the Raman intensity ratio D/G of the peaks at 1350 cm^{-1} (D-band) and 1590 cm^{-1} (G-band) is a good index for the relative defect density in SWCNTs.

3. Results and discussion

3.1. Nitridation of SAMs using N_2 plasma and N_2 neutral beams

Figure 4 shows C (1s) and N (1s) XPS spectra of TP1-SAMs before and after ICP or NB irradiation [18]. Before plasma irradiation, a C (1s) peak was observed around 284.8 eV (figure 4(*a*)) [19]. This peak corresponds to the spectrum of C–C or C–H. No nitrogen peak was observed. After 5 s of ICP irradiation, the C (1s) peak became broader and a new peak appeared at a slightly higher binding energy, which was attributed to the C–N species [19] around 286 eV (figure 4(*b*)). A broader peak around 400 eV also appeared after ICP irradiation. This mainly corresponded to the N–C (from 397.5 eV to 400.3 eV) and N–H (from 398.7 eV to 399.7 eV) peaks (figure 4(*e*)) [19]; the N–C peak could not be clearly separated from the N–H peak. These results indicate that nitrogen was weakly absorbed to the surfaces of the TP1-SAMs as a result of ICP irradiation. However, the integrated C(1s)/Au4(f) ratio decreased to about 66% after ICP irradiation, indicating that energetic ions or UV photons hastened the decomposition of the TP1-SAMs. As a result, the TP1 molecules partially desorbed from the Au surface.

The effect of the NB process on surface nitridation of the TP1-SAMs was also investigated using XPS. The beam energy was maintained at around 10 eV [15], which was equal to the ion energy of the ICP process. After 5 s of NB irradiation, the C (1s) peak shifted to a higher binding energy (around 286 eV), and this shift was attributed to the presence of C–N species (figure 4(*c*)). The peak intensity around 400 eV also increased after N_2 beam irradiation, and the binding energy was almost the same as that observed for the ICP-treated SAMs (figure 4(*f*)). However, unlike the ICP-irradiated SAMs, the integrated C(1s)/Au(4f) peak ratio did not change even after NB irradiation. These results indicate that the surfaces of the TP1-SAMs were modified with nitrogen and no molecular desorption occurred during the NB irradiation. In other words, using the NB process enabled damage-free surface nitridation of the TP1-SAMs by reducing the number of ions and UV photons. However, after 30 s of NB irradiation, the intensity of the sulfur 2 p peak fell to about 60% of the peak observed after 5 s of irradiation. Thus, we conclude that the TP1-SAMs had begun to desorb from the Au substrate after 30 s of NB irradiation.

We used TOF-SIMS to analyse the effect of the NB process on the chemical structure after the surface nitridation of TP1-SAMs. The TOF-SIMS spectra around mass-to-charge

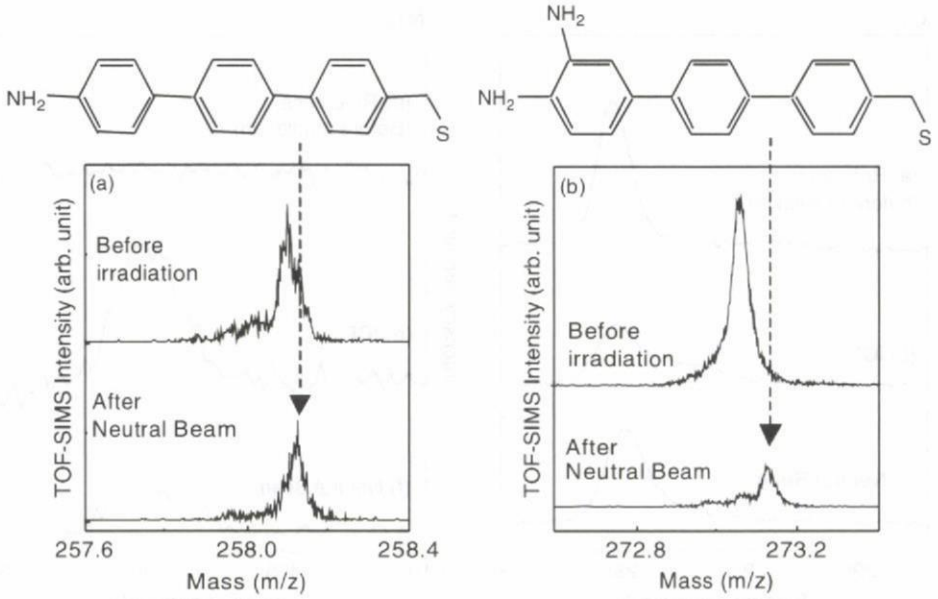

Figure 5. Portions of positive TOF-SIMS spectra of TP1-SAMs before and after NB irradiation [18].

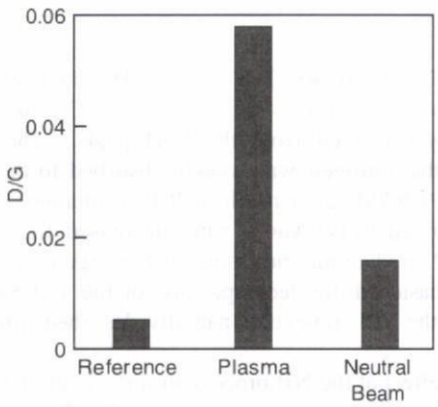

Figure 6. Raman intensity ratio D/G of peaks at 1350 cm^{-1} (D-band) and 1590 cm^{-1} (G-band) in single-walled carbon nanotubes before and after irradiation with Ar plasma and Ar neutral beam. D/G ratio corresponds to relative defect density in SWCNTs.

ratios (m/z) of 258 and 273 are shown in figures 5(a) and (b) [18]. The m/z of 258.12 corresponds to $C_{19}H_{16}N^+$, and the m/z of 273.12 corresponds to $C_{19}H_{17}N_2^+$, whose signals originated from terphenyl methane with one and two NH_2 groups. Before NB irradiation, no $C_{19}H_{16}N^+$ or $C_{19}H_{17}N_2^+$ signals were observed. The spectra indicate that N_2 beam irradiation caused one or two H atoms in the terphenyl group to change into NH_2 groups, and this change is consistent with the N(1s) peak position. Moreover, the TP1-SAMs spectrum remained even after NB irradiation. The intensity of the TP1-SAMs after NB irradiation was about 10% of what it was before. In other words, the TP1-SAMs were reduced by 90%. No other species were observed in the TP1-SAMs after NB irradiation.

During a conventional ICP process, UV photons, rather than highly energetic ions, are the main causes of decomposition and desorption of molecules, because the process generates few energetic ions. The UV photons weaken the chemical bonds between the TP1 molecule and the Au surface, and some of the TP1 molecules then desorb from the Au surface. Furthermore, UV photons can dissociate TP1 molecules. The principles of photochemistry suggest that the benzyl group should be more easily desorbed as a result of photon irradiation [20, 21]. Besides causing these structural changes, nitrogen ions also sputter TP1 molecules and penetrate into TP1 monolayers after partial desorption and decomposition. In contrast, surface nitridation of the TP1-SAMs with the NB process showed no molecular desorption because there were far fewer ions and UV photons. Since desorption due to UV irradiation did not occur, nitrogen could not penetrate the TP1 monolayers. We presume that the nitrogen NB adsorbed only to the TP1 monolayer surface. Thus, this substitution would likely occur only for the top atoms of the terphenyl molecule. The XPS and TOF-SIMS data indicate that one or two H atoms were substituted by NH_2 groups during the NB process. The first NH_2 group probably replaced the top H atom of the terphenyl molecule, and the second NH_2 group may have been located at that position. Since at least one or two excess H atoms are needed for one or two NH_2 substitutions, one unanswered question remains: where did the excess hydrogen come from? We speculate substitution of the hydrogen of the TP1-SAMs into nitrogen is a possible origin. The hydrogen of the remaining CH_2Cl_2 solution on the Au substrate is another possible origin. Hydrogen originating from the H_2O remaining inside the NB chamber is a third possible origin because we observed a peak of H_2O in the NB chamber, even though hydrogen could not be observed during the irradiation when we used a quadrupole mass spectrometer (QMS) to measure the chamber contents during the NB irradiation.

3.2. Surface treatment of SWCNTs using Ar plasma and Ar neutral beam

We evaluated the relative defects density in SWCNTs before and after the plasma and neutral beam irradiation according to the Raman intensity ratio (figure 6). In this experiment, the incident ion energy (about 10 eV) and ion flux (about $6 \times 10^{15}\,\mathrm{cm^{-2}\,s^{-1}}$) from the plasma were almost the same as the incident neutral beam energy and flux in the neutral beam source. The Raman spectra results indicate that Ar neutral beam irradiation did not increase the defects in the SWCNTs, whereas Ar plasma generated a very large number of defects. This suggests that high-energy photons, such as UV and VUV photons during Ar plasma irradiation drastically increased the defects in the SWCNTs.

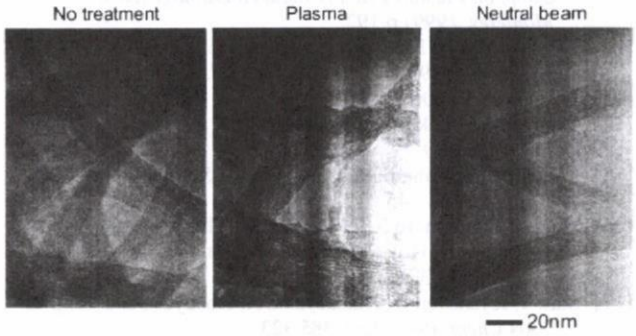

Figure 7. TEM image of carbon nanotubes before and after irradiation with Ar plasma and Ar neutral beam. SWCNT cylinders became rough after plasma irradiation.

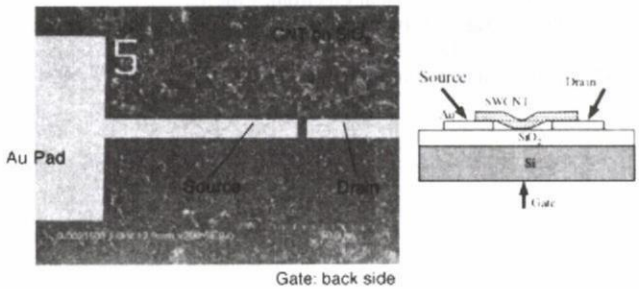

Figure 8. Schematic illustration of carbon nanotube field effect transistor with Au electrode.

Cross-sectional TEM images of SWCNTs before and after Ar plasma or Ar neutral beam treatment are shown in figure 7. The defects generated in the SWCNTs during Ar plasma irradiation can be clearly seen in these images because the cylinder shape is much rougher than before the treatment. Conversely, no defects were observed after we irradiated the SWCNTs with the Ar neutral beam; the SWCNTs had a very smooth cylinder shape. These results show that using our neutral beam method to treat samples produces virtually defect-free atomic layers because the beam is free of UV photons when the beam energy is as low (about 10 eV).

We also observed the electrical characteristics of carbon nanotubes irradiated using Ar plasma and the Ar neutral beam. We fabricated back-gate SWCNT field effect transistors (SWCNT FETs) by using Au pads on SiO_2/Si, as shown in figure 8. The SWCNTs were coated between the source and drain Au electrodes. The voltage (V_{sd}) between the source and drain was fixed at +5 V, and the gate voltage was varied from −10 V to +10 V.

Figure 9 shows the current–voltage (I–V) characteristics of the SWCNT FETs before and after surface treatments with Ar plasma and neutral beams. In the FETs treated with the Ar plasma, the current decreased quickly and the semiconductor characteristics disappeared. In contrast, the I–V characteristics of the FETS treated with the Ar neutral beam at the same bombardment energy remained constant.

These results suggest that the UV and VUV radiation damage (defect generation) strongly influences the electrical characteristics of SWCNTs. Specifically, the larger number of defects caused a drastic increase in the resistance of the SWCNTs. From these results, we found that controlling defects in the carbon nanotube is a very important issue when fabricating nanodevices that contain carbon nanotubes. Furthermore, our neutral beam process is a damage-free top–down process that can be used to fabricate SWCNT FETs.

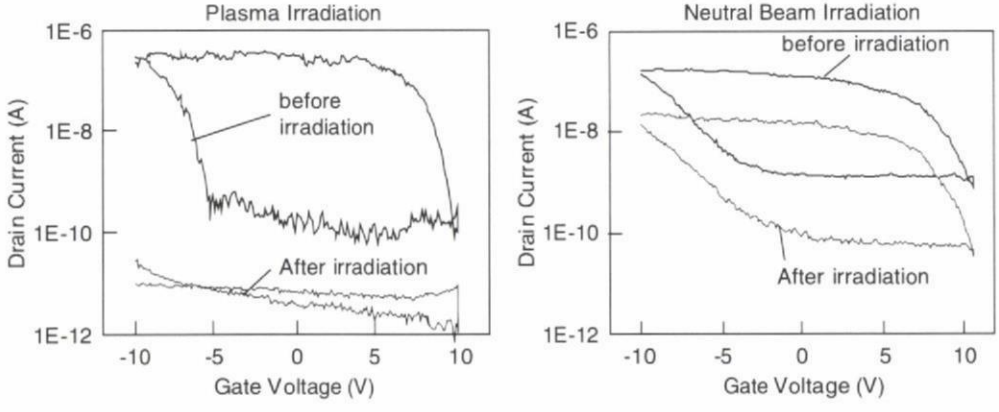

Figure 9. I–V characteristics of carbon nanotubes before and after irradiation with Ar plasma and Ar neutral beam.

4. Conclusion

We found that using the NB process enabled damage-free surface modification of organic monolayers and carbon nanotubes. In contrast, it is very difficult to control the surface nitridation of TP1-SAMs using a conventional ICP process because the TP1-SAMs are easily damaged by UV photon radiation. Additionally, we found that NB treatment of a SWCNT's surface could maintain the bulk structure of the SWCNT, whereas UV irradiation from the Ar plasma generated a large number of defects in the SWCNT. These results suggest that this NB process can provide a damage-free top–down process even for weak materials, such as SAMs and CNTs. The NB process should spur the practical development of future nanoscale devices. Our NB process is a very promising technique for the fusing top–down and bottom–up processes of nanoscale devices.

Acknowledgment

We thank Dr Masahiko Ishida, Dr Fumiyuki Nihey and Dr Yukinori Ochiai of NEC Corporation for their useful advice, discussions and sample supply.

References

[1] Nozawa T and Kinoshita T 1995 *Japan. J. Appl. Phys.* **34** 2107
[2] Kinoshita T, Hane M and McVittee J P 1996 *J. Vac. Sci. Technol.* B **14** 560
[3] Ootera H 1993 *Japan. J. Appl. Phys.* **33** 6109
[4] Ohtake H and Samukawa S 1995 *Proc. 17th Dry Process Symp. (Institute of Electrical Engineering of Japan, Tokyo, 1995)* p 45
[5] Okamaoto T, Ide T, Sasaki A, Azuma K and Nakata Y 2004 *Japan. J. Appl. Phys.* **43** 8002
[6] Yonekura K, Goto K, Mastuura M, Fujiwara N and Tsujimoto K 2005 *Japan. J. Appl. Phys.* **44** 2976
[7] Cheung K P and Pai C S 1995 *IEEE Electron Device Lett.* **16** 220
[8] Carrere J-P, Oberlin J-C and Haond M 2000 *Proc. Int. Symp. on Plasma Process-Induced Damage (AVS, Monterey, 2000)* p 164
[9] Dao T and Wu W 1996 *Proc. Int. Symp. on Plasma Process-Induced Damage (AVS, Monterey, 1996)* p 54
[10] Joshi M, McVittee J P and Sarawat K 2000 *Proc. Int. Symp. on Plasma Process-Induced Damage (AVS, Monterey, 2000)* p 157
[11] Cismura C, Shohet J L and McVittee J P 1999 *Proc. Int. Symp. on Plasma Process-Induced Damage (AVS, Monterey, 1999)* p 192
[12] Woodworth J R, Blain M G, Jarecki R L, Hamilton T W and Aragon B P 1999 *J. Vac. Sci. Technol.* A **17** 3209
[13] Samukawa S 2006 *Japan. J. Appl. Phys.* **45** 2395
[14] Samukawa S, Sakamoto K and Ichiki K 2001 *Japan. J. Appl. Phys.* **40** L779
[15] Samukawa S, Minemura Y and Fukuda S 2004 *J. Vac. Sci. Technol.* A **22** 245
[16] Ishida T, Yamamoto S-I, Mizutani W, Motomatsu M, Tokumoto H, Hokari H, Azehara H and Fujihira M 1997 *Langmuir* **13** 3261
[17] Sato Y, Jeyadeven B, Hatakeyama R, Kasuya A and Tohji K 2004 *Chem. Phys. Lett.* **385** 323
[18] Ishikawa Y, Ishida T and Samukawa S 2006 *Appl. Phys. Lett.* **89** 123122
[19] Moulder J F, Stickle W F, Sobol P E and Bomben K D 1995 *Handbook of X-ray Photoelectron Spectroscopy* (Minnesota: Physical Electronics Inc.)
[20] Ishida T, Sano M, Fukushima H, Ishida M and Sasaki S 2002 *Langmuir* **18** 10499
[21] Gazith M and Noyes R M 1955 *J. Am. Chem. Soc.* **77** 6091

CARBON 46 (2008) 1927–1934

available at www.sciencedirect.com

ScienceDirect

journal homepage: www.elsevier.com/locate/carbon

In vivo rat subcutaneous tissue response of binder-free multi-walled carbon nanotube blocks cross-linked by de-fluorination

Yoshinori Sato[a,], Atsuro Yokoyama[b,*], Takao Kasai[b], Shinji Hashiguchi[c], Makoto Ootsubo[a], Shin-ichi Ogino[a], Naoki Sashida[a], Masaru Namura[a], Kenichi Motomiya[a], Balachandran Jeyadevan[a], Kazuyuki Tohji[a]*

[a]*Graduate School of Environmental Studies, Tohoku University, Aoba 6-6-20, Aramaki, Aoba-ku, Sendai 980-8579, Japan*
[b]*Graduate School of Dental Medicine, Hokkaido University, Kita 13, Nishi 7, Kita-ku, Sapporo 060-8586, Japan*
[c]*Stella Chemifa Co., 1-41 Rinkai-cho, Izumiotsu, Osaka 595-0075, Japan*

ARTICLE INFO

Article history:
Received 22 May 2008
Accepted 2 August 2008
Available online 12 August 2008

ABSTRACT

Binder-free multi-walled carbon nanotube (MWCNT) blocks from fluorinated MWCNTs were prepared using thermal heating and a compression method in vacuo. The resulting carbon nanotube blocks are lighter than graphite, can be machined and polished, possess average bending strengths of 102.2 MPa, a bending modulus of 15.4 GPa, and moderate wettability. The binder-free MWCNT blocks possess good biocompatibility when tested in the subcutaneous tissue of rats in vivo, which were covered by thin granulation tissue, 40–70 μm in thickness, comprising a few lymphocytes, cell with large cytoplasmic spaces like fibroblasts and foreign-body giant cells. That is indicative of a slight inflammatory response than MWCNT/resin blocks and poly(methyl methacrylate). This material can potentially be employed as an alternative artificial hard tissue or internal bone plate that makes use of the properties of CNTs.

1. Introduction

Since the excellent antithrombotic property of graphite was discovered in 1963 [1], biocompatible artificial organs or internal bone plates have been developed using carbon materials such as low temperature isotropic carbon (LIT) [2,3] in high density isotropic carbon materials, carbon fiber-reinforced carbon composites (C/C) [4–8] and polymer/carbon fiber composites [9,10]. In particular, C/C have been used as an alternative hard tissue material of bone or dental root, which have been generated from carbon fibers (CFs) and resins by a combination of resin impregnation and hot press methods. Graphite and traditional C/C materials have been solidified by graphitization of a resin (binder) and possess an apparent density, 2.0–2.2 g/cm^3. Over the past several years, basic biomedical research concerning drug delivery [11–13] and the use of scaffolds [14–18] and catheters [19,20] has been carried out using a new type of carbon allotrope comprising carbon nanotubes (CNTs). We have investigated the use of alternative artificial hard tissue materials comprising CNT composites [21,22]. As CNTs possess low density, high mechanical strength [23] and protein adsorption properties [24,25], artificial hard tissue alternative materials comprising CNTs can potentially be utilized as lightweight, porous, and strong three-dimensional materials [26] composed of one-dimensional CNTs that offer advantages in comparison with the use of graphite and traditional C/C materials. Recently, we have produced large-sized binder-free multi-walled carbon

* *Corresponding authors:* Fax: +81 22 795 3868 (Y. Sato); +81 11 706 4903 (A. Yokoyama).
E-mail addresses: hige@bucky1.kankyo.tohoku.ac.jp (Y. Sato), yokoyama@den.hokudai.ac.jp (A. Yokoyama).
0008-6223/$ - see front matter © 2008 Elsevier Ltd. All rights reserved.
doi:10.1016/j.carbon.2008.08.003

nanotube (MWCNT) blocks from fluorinated MWCNTs using thermal heating and a compression method in vacuo (the blocks are referred to as "de-F-MWCNT blocks") [27]. This technique resulted in the formation of covalent MWCNT networks generated by the introduction of sp^3-hybridized carbon atoms that cross-link between nanotubes following de-fluorination. The resulting CNT blocks have a low apparent density 1.44 g/cm^3 derived from solidification of pure MWCNT in the absence of a binder, can be machined and polished, and possess average three times stronger mechanical strength, bending strengths of 102.2 MPa and a bending modulus of 15.4 GPa, than that of commercial graphite. Thus, the de-F-MWCNT blocks are light and strong, and can potentially be employed for use as alternative artificial hard tissue materials in biomedical application.

Biomaterials need to possess: (a) lightweight, mechanical strength, decay durability, abrasion-proof and fatigue-resistant properties and (b) antithrombogenicity, adhesion to body tissue, corrosion fatigue resistance and biocompatibility. The most critical factor concerns the biocompatibility of materials. Generally, use of the "implant test in vivo" [28], the most important and basic toxic evaluation method, is employed to examine material responses to tissue in vivo as well as cellular responsive reactions in vitro. Here, we report on the tissue response of binder-free de-F-MWCNT blocks following subcutaneous implant in rats to evaluate their biocompatibility comparing with MWCNT/resin blocks carbonized with 50 wt% phenol resin, poly(methyl methacrylate) (PMMA; negative control), and pure Ni metal (positive control) as reference materials.

2. Materials and methods

2.1. Purification of MWCNTs

The purity of the MWCNTs was ca. 80 wt%, and the rest of the material consisted of amorphous carbon (8.50 wt%), Al (5.73 wt%), Fe (4.43 wt%), Mo (1.27 wt%) and Cr (0.07 wt%). The nanotubes exhibited bamboo-like morphologies. The average tube diameter ranged from 20 to 40 nm, and the lengths ranged from 500 nm to 5.0 μm. The MWCNT soot was burned in air at 773 K for 90 min and the remaining soot was then introduced into a flask containing 6 M-HCl in order to dissolve the Fe, Mo and Cr. Following this procedure, the acid solution was filtered using a membrane filter, and 1.0 g of the filtered material was transferred into a flask with 1.0 L of 2 M-NaOH and refluxed at 373 K for 6 h in order to dissolve aluminum oxides. The resulting suspension was then filtered and washed with hot water. Finally, samples were dried in vacuo at 373 K for 24 h. Following purification, the impurities consisted of Na (0.40 wt%), Al (1.41 wt%), Fe (0.26 wt%), Mo (1.27 wt%) and Cr (0.15 wt%). The elemental analysis was obtained using inductively coupled plasma optical emission spectroscopy (ICP-OES).

2.2. Fluorination of MWCNTs

Purified MWCNTs (150 mg) were fluorinated at 523 K using a mixture of F_2 (20%) and N_2 (80%) for 2 h (flow rate of 25 mL/min). Thermal annealing was then carried out at 523 K for 6 h in a polytetrafluoroethylene cell under a nitrogen flow of 20 mL/min. We repeated this fluorination procedure several times. The products were then characterized by X-ray photoelectron spectroscopy (XPS) using an AXIS-His (Kratos Analytical Ltd., UK), and the C:F stoichiometries were determined.

2.3. Preparation of de-F-MWCNT blocks

The de-F-MWCNT blocks were prepared using a SPS system (Sumitomo Coal Mining, SPS-1050, Japan). The SPS systems is a unique synthesis and processing technique which allows for sintering at low temperatures and short periods of time by charging particles with electrical energy, and effectively applying the high energy of a spark plasma. The SPS process possesses very high thermal efficiency because of the direct heating caused by the spark, and can readily produce a homogeneous, high-quality sintered product due to the uniform heating generated. Typically, 300 mg of the MWCNT powder was used and hardened in a graphite mold with a diameter of 20 mm at 1273 K (heating rate: 25 K/min), under a pressure of 80 MPa in vacuo (1×10^{-2} Torr) for 10 min. The resulting sample was 20 mm in diameter and 2.0 mm in thickness. The typical weight loss of de-F-MWCNT blocks was 50.0–55.3 wt% of the initial fluorinated MWCNT powder.

2.4. Preparation of MWCNT/resin blocks

Purified MWCNTs (500 mg) was mixed with 500 mg of the phenol resin in 100 mL of ethanol at 298 K, sonicated for 1 h, and the ethanol was then evaporated at 333 K. Thermal annealing was then carried out at 773 K for 2 h in an alumina boat under a nitrogen flow of 20 mL/min in an effort to carbonize the phenol resin. In a similar manner as with the production of de-F-MWCNT blocks, 300 mg of the MWCNT powder was used and hardened in a graphite-covered die with a diameter of 20 mm at 1273 K (heating rate: 25 K/min), under a pressure of 80 MPa in vacuo (1×10^{-2} Torr) for 10 min. The resulting sample was 20 mm in diameter and ~2.0 mm in thickness. The weight loss of MWCNT/resin blocks was 5.0–10 wt% of the initial MWCNT/carbonized resin powder.

2.5. Analysis of materials

The sample morphologies were determined by scanning electron microscopy (SEM; S-4100, Hitachi, Japan) and high-resolution transmission electron microscopy (HRTEM; HF-2000, Hitachi, Japan) equipped with a field emission gun. SEM and HRTEM were operated at 5 and 200 kV, respectively. The HRTEM was equipped with a NORAN Instruments energy-dispersive X-ray detector and a Gatan imaging filter with an energy resolution of 1.0 eV. Metal impurities were detected by ICP-OES (Thermo elemental Co., Ltd., USA). The vibrational modes of the modified nanotube samples were characterized using Fourier transform-infrared absorption spectroscopy (FT-IR; Avatar 380, Thermo Electron Co., Ltd., USA). The samples were measured inside a KBr pellet. Water contact angles of the samples were measured using a contact angle meter (face CA-DS, Kyowa Interface Science Co., Ltd., Japan). The flaked particles from the sample blocks in distilled water were

measured using a particle counter (KL-27, RION Co., Ltd., Japan). For the contact angle and particle count measurements, the shape of the specimens tested was approximately $2.0 \times 1.0 \times 8$ mm. The blocks were polished with Emery paper (# 1200) and Fuji film lapping tape (# 2000 and # 4000) (Fuji Photo Film Co., Ltd., Japan). The mechanical properties of the solid blocks, the Young's modulus and fracture strength were measured using three-point bending tests, which were performed on a universal testing machine (Instron 5582) at atmospheric conditions and room temperature. The load was applied at a cross-head speed of 0.05 mm/min. The Young's modulus E_b and fracture strength σ_b were calculated as previously described. Three specimens were tested, and the averaged results were obtained. The shape of the specimens tested was approximately $2.0 \times 1.0 \times 18$ mm. The solid specimens were polished with Emery paper (# 1200) and Fuji film lapping tape (# 2000 and # 4000) (Fuji Photo Film Co., Ltd., Japan). Eight tests were performed on each material.

2.6. *Inflammatory response to MWCNT blocks and reference sample*

The shape of the de-F-MWCNT and MWCNT/resin blocks was $1.0 \times 1.0 \times 10$ mm, and that of PMMA and pure Ni metal (99.9%, Niraco Co., Japan) was $1.6 \times 1.9 \times 5.4$ and $0.7 \times 1.0 \times 6.6$ mm, respectively. All blocks were polished with Emery paper (# 1200) and Fuji film lapping tape (# 2000 and # 4000) (Fuji Photo Film Co., Ltd., Japan) and sonicated with distilled water to remove the polished powder. Six male 6-week-old Wistar strain rats were used in this study. Incisions were made bilaterally in the thoracic region under general anesthesia. Two pockets were made in the subcutaneous tissue. A block was implanted in the subcutaneous tissue in the thoracic region bilaterally in each rat. Animal experiments were performed in accordance with the Guide for the Care and Use of Laboratory Animals, Hokkaido University Graduate School of Dental Medicine. No rats were lost during the course of this study. Three numerical values were acquired for each condition.

2.7. *Histological procedure and observation by optical microscopy*

One week following surgery, segments of subcutaneous tissue including sample were excised, fixed and then embedded in paraffin. Hematoxylin and eosin-stained specimens were observed by optical microscopy (AX80, Olympus, Japan).

3. Results and discussion

The apparent density of the de-F-MWCNT blocks is 1.44 g/cm^3, and the fracture bending strength and Young's modulus (bending modulus) of the de-F-MWCNT blocks were on average 102.2 MPa (min 92.4 MPa, max 122.7 MPa) and 15.4 GPa, respectively (Table 1). The de-F-MWCNT blocks are light, possess excellent mechanical strength and are able to be manufactured and polished (Fig. 1a). The MWCNTs were found to be embedded in the whole cross-section (Fig. 1b). As can be seen on the fracture surface, each individual MWCNT was observed and seemed to have excellent contact along the nanotube axis. Other carbon materials were notably absent under the present conditions. The fracture bending strength and Young's modulus of the de-F-MWCNT blocks were 2.1 and 1.5 times larger, respectively, than those of MWCNT/resin blocks due to the cross-linking of each nanotube by de-fluorination [27].

Given that in biomaterials nanosize particles derived from abrasion, wear, or polish debris particles can cause inflammation [29–31], we measured a particle broken off from the de-F-MWCNT blocks immersed in distilled water (Fig. 2a). A particle analyzer is able to detect over 300 nm size particles. In the de-F-MWCNT blocks, particles were detected to be 11.9 (particle/mL) after 1 h and 8.7 (particle/mL) after 72 h, and demonstrating no difference with that of distilled water and PMMA. This indicates that there are few abrasions with particle sizes over 300 nm from the de-F-MWCNT blocks infiltrated in distilled water. Fig. 2b shows the contact angle of the sample for distilled water. Artificial blood vessels need to be antithrombogenic and show no protein adsorption. However, as artificial hard tissue alternative materials need to adhere closely to cells and tissues at the material interface, it is desirable that these materials possess hydrophilicity. The contact angle of the de-F-MWCNT blocks is 42.0°, which represents high hydrophilicity in comparison with that of PMMA. This indicates that the de-F-MWCNT blocks possess a suitable surface that could be utilized in artificial bone and dental root applications.

Soft tissue inflammatory responses to artificial materials are important at the early implantation stage. As time passes, the vicinity occupied by the artificial material is covered with granulation tissue comprising lymphocytes, cell with large cytoplasmic spaces like fibroblasts, macrophages, and fibroblasts that restore tissue grow vigorously with the onset of fibrosis. As more time passes, artificial materials are covered by a fibrous capsule. Therefore, the extent of the inflammatory response to artificial materials is indicated by the thickness of the granulation tissue, the number, type and distribution of polymorphonuclear leukocytes, lymphocytes, cell with large cytoplasmic spaces like fibroblasts, fibroblasts, foreign-body giant cells, and macrophages observed in the tissue [28]. Table 2 shows the thickness of the granulation tissue and cell types present in the granulation tissue at 1 week after surgery. Low- and high-magnification histological

Table 1 – Mechanical properties of CNT blocks

Characteristic	de-F-MWCNT blocks	MWCNT/resin blocks
Bulk density p (g/cm^3)	1.44	1.41
Youngs modulus E_b (GPa)	14.2–16.3	8.7–10.7
Fracture bending strength a_b (MPa)	92.4–123.0	41.2–56.1

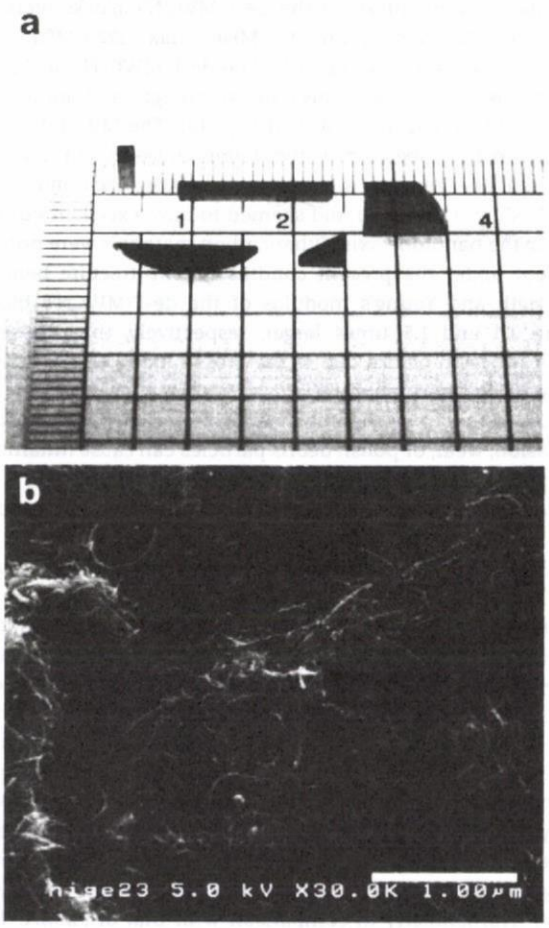

Fig. 1 – (a) Image showing variously shaped de-F-MWCNT blocks and (b) high-magnification SEM image of the fracture surface of the de-F-MWCNT blocks (scale bar; 1.0 μm).

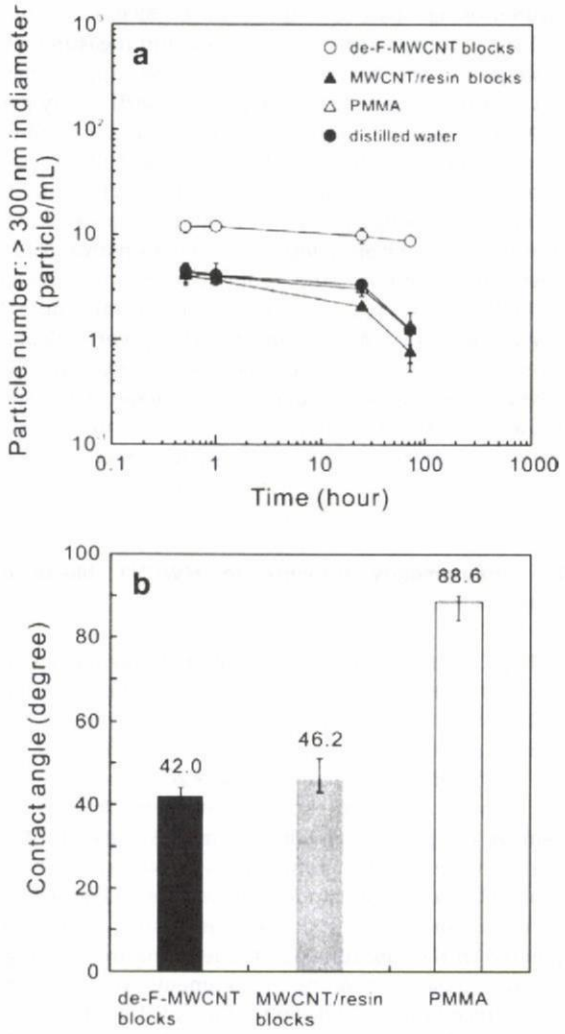

Fig. 2 – (a) Particle number (with size greater than 300 nm) from the samples infiltrated in distilled water as a function of time. de-F-MWCNT blocks (○), MWCNT/resin blocks (▲), and PMMA (△). The reference is distilled water. (b) Contact angle of sample for distilled water.

optical microscope images of each sample implanted in the subcutaneous tissue at 1 week after surgery are shown in Figs. 3 and 4. Asterisk (*) is the place where samples were implanted. The de-F-MWCNT blocks were covered by thin granulation tissue, 40–70 μm in thickness, comprising a few lymphocytes, cell with large cytoplasmic spaces like fibroblasts and foreign-body giant cells, which is indicative of a slight inflammatory response (Figs. 3 and 4a). On the other hand, in the MWCNT/resin blocks, a thick granulation tissue 290–340 μm in thickness was observed (Fig. 3b), comprising many lymphocytes, cell with large cytoplasmic spaces like fibroblasts and macrophages, in addition to dilatation of blood capillaries. This inflammation was greater than that observed with the de-F-MWCNT blocks. Macrophages and foreign-body giant cells positioned at the interface of the de-F-MWCNT blocks and MWCNT/resin blocks may be involved in the phagocytosis of a small number of less than 300 nm fragments detached from the blocks (Fig. 4b). The thickness of the granulation tissue surrounding PMMA was observed to be in the range between 40 and 120 μm (Fig. 3c), in which immature fibroblasts, macrophages, eosinophils and the dilatation of blood capillaries were observed (Fig. 4c). We found that the inflammation response to PMMA was moderately stronger than that of the de-F-MWCNT blocks, but weaker compared with that response observed for the MWCNT/resin blocks. The inflammatory response to the pure Ni metal positive control was strong, as indicated by the many macrophages, neutrophils, necrosed tissue (no nuclei, light pink color) and diapedesis of red blood cells that were observed (Figs. 3 and 4d) [32]. Thus, the de-F-MWCNT blocks were found to be associated with little acute inflammation and promising biocompatibility in the soft tissue given our examination of the thin granulation tissue. The biocompatibility of titanium [33] and hydroxyapatite [34] has been reported in terms of soft tissue responses in vivo with a view to establishing the efficacy of employing these biomaterials as bone supply materials and dental implants. Inflammatory responses to titanium and hydroxyapatite ceramics in soft tissue differ only slightly in comparison to the responses observed to de-F-MWCNT blocks, which are covered by thin fibrous connec-

Table 2 – Thickness of granulation tissue and cell types in the granulation tissue

Materials	Granulation tissue thickness (μm)	Cells inducted by materials in granulation tissue
de-F-MWCNT blocks	40–70	Lymphocyte Cells with large cytoplasmic spaces like fibroblasts Fibroblast Foreign body giant cell
MWCNT/resin blocks	290–340	Lymphocyte Cells with large cytoplasmic spaces like fibroblasts Blood capillary Macrophage
PMMA	40–120	Macrophage Eosinophil Fibroblast Blood capillary Foreign body giant cell
Ni	300–1000	Necrotic cell Macrophage Neutrophil Blood capillary Red blood cell

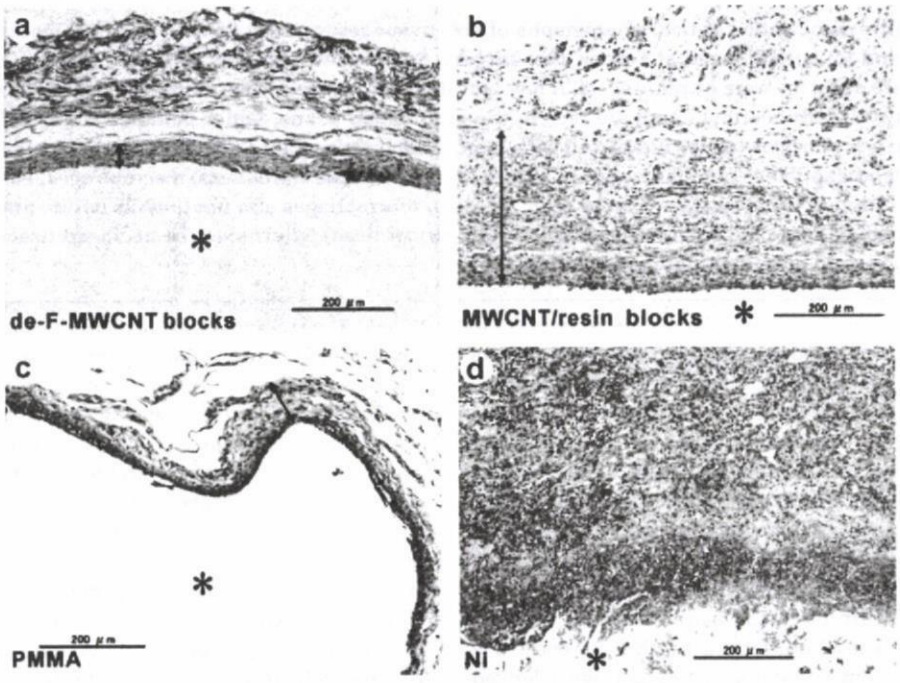

Fig. 3 – Typical low-magnification optical photographs of soft tissue response to (a) de-F-MWCNT blocks, (b) MWCNT/resin blocks, (c) PMMA, and (d) pure Ni metal at 1 week after surgery. Samples were stained with hematoxylin and eosin. Asterisk (*) is the place where samples were implanted. Arrow span shows granulation tissue thickness. In the case of pure Ni metal, necrosed tissue was observed.

tive tissue at the early implantation stage. However, as hydroxyapatite cement [35] or hydroxyapatite [36] synthesized by spark plasma sintering method show the same tissue response as that elicited with the use of de-F-MWCNT blocks, the latter seem to possess sufficient biocompatibility.

The in vivo tissue response to pure MWCNTs [37,38], MWCNTs with carboxyl groups [39] and hat-stacked carbon nanofibers [40] as determined from histological and high-resolution transmission electron microscope (HRTEM) observations suggest the absence of an acute inflammatory response. Although in vivo tests using CN_x nanotubes [41,42], in vitro and in vivo tests of various functionalized CNTs [43,44] and carbon nanohorn [45] have shown these materials to be biocompatible, use of MWCNT/resin blocks

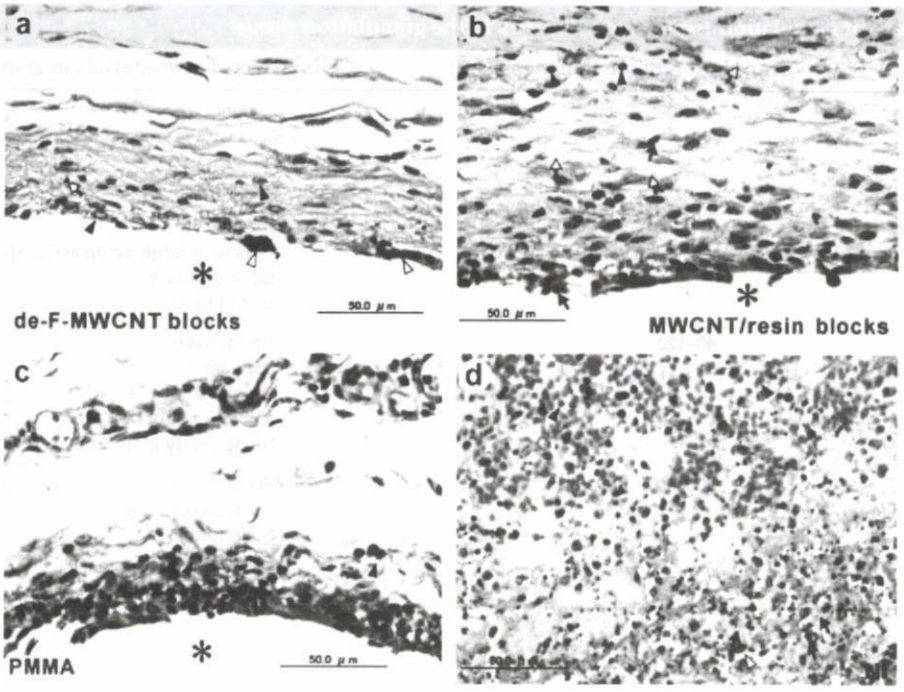

Fig. 4 – Typical high-magnification optical photographs of soft tissue response to (a) de-F-MWCNT blocks, (b) MWCNT/resin blocks, (c) PMMA, and (d) pure Ni metal at 1 week after surgery. Samples were stained with hematoxylin and eosin. Asterisk (*) is the place where samples were implanted. (a) A few lymphocytes (white arrow), immature fibroblasts (arrow head), and foreign-body giant cells (white arrow head) are seen in the granulation tissue, which is indicative of a slight inflammatory response. (b) Many lymphocytes (arrow head), cell with large cytoplasmic spaces like fibroblasts, macrophages (arrow), and the dilatation of blood capillaries (white arrow) are observed. (c) Immature fibroblasts, macrophages, eosinophils (arrow head), and the dilatation of blood capillary can be seen. (d) Many macrophages and neutrophils (white arrow head), necrosed tissue (arrow; no nuclei, light pink color) and red blood cells (arrow head) external to the necrosed tissue appear. The inflammatory response to pure Ni metal is very strong.

elicits an inflammatory response. Aircraft production workers exposed to resin containing C/C have developed dermatitis [46]. In our case, although there is no amorphous carbon in the purified MWCNTs, amorphous carbon is present in the MWCNT/resin blocks as determined by HRTEM observations (Figs. S1 and S2), which indicates that phenol resins were carbonized. The presence of functional groups on the de-F-MWCNT blocks and MWCNT/resin blocks was established by FT-IR spectroscopy using a transmission method (KBr pellet). The FT-IR spectrum of carbon nanotubes with a higher defect concentration is characterized by the presence of a broader band at 1220 cm^{-1} that is assigned to a signal derived from the carbon skeleton [47,48], and the band present at 1584 cm^{-1} in the two spectra is associated with the stretching vibration of the aromatic C=C group (Fig. S3). The band assigned to the C–F covalent bond is absent in the FT-IR spectrum of the de-F-MWCNT blocks, while a broader band located at 1203 cm^{-1} and assigned to the carbon skeleton is present [27]. On the other hand, in the MWCNT/resin blocks, the slight bands at 2844 and 2921 cm^{-1} assigned to the stretching vibration of the C–H group are present (Fig. S3). However, the presence of the phenol is not reliable because of poor IR absorption. Recently, Lison and Fubini groups [49,50] have investigated the effect of the presence of CNT framework and surface defects on lung toxicity of MWCNTs. They explored the physicochemical determinants of these toxic responses with progressively and selectively modified CNTs (i) by grinding (introducing structural defects) and heating either in a vacuum at 873 K (causing reduction of oxygenated carbon functionalities and reduction of oxidized metals) or in an inert atmosphere at 2673 K (causing elimination of metals and annealing of defects) and (ii) by heating at 2673 K in an inert atmosphere and grinding the thermally treated MWCNTs (introducing defects in a metal-deprived carbon framework). In vivo and vitro experiments performed to evaluate lung response in bronchoalveolar lavage fluid (lactase dehydrogenase (LDH), proteins, cellar infiltration, interleukin-1 beta (IL-1β), and tumor necrosis factor-alpha (TNF-α)) using Wistar rats and to assess the genotoxic potential of the modified CNTs cytokinesis block micronucleus assay, respectively. From the physicochemical aspects, the potential of the modified CNT to scavenge hydroxyl radicals was evaluated by means of electron spin resonance spectroscopy. The results show that acute pulmonary toxicity and the genotoxicity of CNT were reduced upon heating but restored upon grinding. In addition, the original ground MWCNTs exhibited a scavenging activity toward hydroxyl radicals, which was eliminated by heating at 2673 K but restored upon grinding. This scavenging activity, related to the presence of defects, appears to go paired with the genotoxic and inflammatory

potential of MWCNT. They conclude that the intrinsic toxicity of CNT is mainly mediated by the presence of defective sites in their carbon framework. From the point of view of the presence of defective carbon materials, in the MWCNT/resin blocks, the inflammation response might be accounted for by the presence of amorphous carbon-like unidentified carbon frameworks that remain due to imperfect carbonization of the resin.

4. Conclusion

We found that the binder-free MWCNT blocks cross-linked by de-fluorination possess biocompatibility as assessed following the in vivo implantation of rats. As this block is light, strong, and biocompatible, it can be applied to internal bone plates [51] or bone. In the latter application, a critical issue concerning the use of carbon composite materials as an alternative hard tissue material has to do with the lack of strongly adhering tissue to the carbon materials. However, it is hoped that the use of CNTs can obviate this problem. For example, we found that osteoblasts tightly adhered to a scaffold comprising CNT [15,17]. Additionally, CNTs are able to bind [52], immobilize [53,54], and trap proteins [24,25], and hydroxyapatite separates out on the surface of CNTs [18,38,55,56]. If three-dimensional highly porous carbon nanotube blocks in which cells could live could be prepared by the method for producing active cross-linking sites on nanotube surfaces via de-fluorination of multi-walled carbon nanotubes, carbon nanotube biomaterials onto which tissue can tightly adhere might be designed using a combination of protein, hydroxyapatite and CNTs.

Acknowledgments

This work was supported by a Grant-in-Aid for Young Research (A) 19686038, and Exploratory Research 19656175 from the Ministry of Education, Science, Culture and Sport of Japan, and Health and Labor Sciences Research Grant No. H18-chemistry-006 from the Ministry of Health, Labor and Welfare.

Appendix A. Supplementary material

TEM image of MWCNT/resin blocks (Fig. S1), elemental analysis of amorphous carbon of MWCNT/resin blocks by TEM-EDX (Fig. S2), and functional group analysis of de-F-MWCNT and MWCNT/resin blocks by FT-IR (Fig. S3).

Supplementary data associated with this article can be found, in the online version, at doi:10.1016/j.carbon.2008.08.003.

REFERENCES

[1] Gott VL, Whiffen JD, Dutton RC. Heparin bonding on colloidal graphite surfaces. Science 1963;142:1297–8.
[2] Bokros JC. Carbon biomedical devices. Carbon 1977;15:355–71.
[3] Hulbert SF, Bokros JC. Use of carbons in dental and orthopedic implants. Carbon 1977;15:429.
[4] Makisalo S, Paavolainen P, Gronblad M, Holmstrom T. Tissue reactions around two alloplastic ligament substitute materials: experimental study on rats with carbon fibres and polypropylene. Biomaterials 1989;10:105–8.
[5] Demmer P, Fowler M, Marino AA. Use of carbon-fibers in the reconstruction of knee ligaments. Clin Orthop Relat Res 1991;271:225–32.
[6] Brüchmann H, Huttinger KJ. Carbon, a promising material in endoprosthetics. Part 1: the carbon materials and their mechanical properties. Biomaterials 1980;1:67–72.
[7] Howling GI, Sakoda H, Antonarulrajah A, Marrs H, Stewart TD, Appleyard S, et al. Biological response to wear debris generated in carbon based composites as potential bearing surfaces for artificial hip joints. J Biomed Mater Res B 2003;67:758–64.
[8] Howling GI, Ingham E, Sakoda H, Stewart TD, Fisher J, Antonarulrajah A, et al. Carbon–carbon composite bearing materials in hip arthroplasty: analysis of wear and biological response to wear debris. J Mater Sci Mater Med 2004;15:91–8.
[9] Jenkins GM, de Carvalho FX. Biomedical applications of carbon fibre reinforced carbon in implanted prostheses. Carbon 1977;15:33–7.
[10] Slivka MA, Chu CC, Adisaputro IA. Fiber–matrix interface studies on bioabsorbable composite materials for internal fixation of bone fractures. 1. Raw material evaluation and measurement of fiber–matrix interfacial adhesion. J Biomed Mater Res 1997;36:469–77.
[11] Pantarotto D, Singh R, McCarthy D, Erhardt M, Briand JP, Prato M, et al. Functionalized carbon nanotubes for plasmid DNA gene delivery. Angew Chem Int Ed 2004;43:5242–6.
[12] Kam NWS, Liu Z, Dai H. Carbon nanotubes as intracellular transporters for proteins and DNA: an investigation of the uptake mechanism and pathway. Angew Chem Int Ed 2004;45:577–81.
[13] Lu Q, Moore JM, Huang G, Mount AS, Rao AM, Larcom LL, et al. RNA polymer translocation with single-walled carbon nanotubes. Nano Lett 2004;4:2473–7.
[14] Correa-Duarte MA, Wagner N, Rojas-Chapana J, Morsczeck C, Thie M, Giersig M. Fabrication and biocompatibility of carbon nanotube-based 3D networks as scaffolds for cell seeding and growth. Nano Lett 2004;4:2233–6.
[15] Aoki N, Yokoyama A, Nodasaka Y, Akasaka T, Uo M, Sato Y, et al. Cell culture on a carbon nanotube scaffold. J Biomed Nanotechnol 2005;1:402–5.
[16] Lovat V, Pantarotto D, Lagostena L, Cacciari B, Grandolfo M, Righi M, et al. Carbon nanotube substrates boost neuronal electrical signaling. Nano Lett 2005;5:1107–10.
[17] Aoki N, Yokoyama A, Nodasaka Y, Akasaka T, Uo M, Sato Y, et al. Strikingly extended morphology of cells grown on carbon nanotubes. Chem Lett 2006;35:508–9.
[18] Zanello LP, Zhao B, Hu H, Haddon RC. Bone cell proliferation on carbon nanotubes. Nano Lett 2006;6:562–7.
[19] Endo M, Koyama S, Matsuda Y, Hayashi T, Kim YA. Thrombogenicity and blood coagulation of a microcatheter prepared from carbon nanotube-nylon-based composite. Nano Lett 2005;5:101–5.
[20] Koyama S, Haniu H, Osaka K, Koyama H, Kuroiwa N, Endo M, et al. Medical application of carbon-nanotube-filled nanocomposites: the microcatheter. Small 2006;2:1406–11.
[21] Wang W, Watari F, Omori M, Liao S, Zhu YH, Yokoyama A, et al. Mechanical properties and biological behavior of carbon nanotube/polycarbosilane composites for implant materials. J Biomed Mater Res B 2007;82:223–30.
[22] Wang W, Omori M, Watari F, Yokoyama A. Novel bulk carbon nanotube materials for implant by spark plasma sintering. Dent Mater J 2004;24:478–86.

[23] Yu MF, Lourie O, Dyer MJ, Moloni K, Kelly TF, Ruoff RS. Strength and breaking mechanism of multiwalled carbon nanotubes under tensile load. Science 2000;287:637–40.
[24] Lin Y, Allard LF, Sun YP. Protein-affinity of single-walled carbon nanotubes in water. J Phys Chem B 2004;108:3760–4.
[25] Salvador-Morales C, Flahaut E, Sim E, Sloan J, Green MLH, Sim RB. Complement activation and protein adsorption by carbon nanotubes. Mol Immunol 2006;43:193–201.
[26] Romo-Herrera JM, Terrones M, Terrones H, Dag S, Meunier V. Covalent 2D and 3D networks from 1D nanostructures: designing new materials. Nano Lett 2007;7:570–6.
[27] Sato Y, Ootsubo M, Yamamoto G, Van Lier G, Terrones M, Hashiguchi S, et al. Super-robust, lightweight, conducting carbon nanotube blocks cross-linked by de-fluorination. ACS Nano 2008;2:348–56.
[28] Shankar R, Greisler HP. In: Greco RS, editor. Implantation biology: the host response and biomedical devices. Boca Raton: CRC Press; 1994. p. 67–80.
[29] Tamura K, Takashi N, Kumazawa R, Watari F, Totsuka Y. Effects of particle size on cell function and morphology in titanium and nickel. Mater Trans 2002;43:3052–7.
[30] Oberdörster G, Stone V, Donaldson K. Toxicology of nanoparticles: a historical perspective. Nanotoxicology 2007;1:2–25.
[31] Lewinski N, Colvin V, Drezek R. Cytotoxicity of nanoparticles. Small 2008;4:26–49.
[32] Uo M, Watari F, Yokoyama A, Matsuno H, Kawasaki T. Tissue reaction around metal implants observed by X-ray scanning analytical microscopy. Biomaterials 2001;22:677–85.
[33] Matsuno H, Yokoyama A, Watari F, Uo M, Kawasaki T. Biocompatibility and osteogenesis of refractory metal implants, titanium, hafnium, niobium, tantalum and rhenium. Biomaterials 2001;22:1253–62.
[34] MacNeill SR, Cobb CM, Rapley JW, Glaros AG, Spencer P. In vivo comparison of synthetic osseous graft materials – a preliminary study. J Clin Periodontol 1999;26:239–45.
[35] Yokoyama A, Matsuno H, Yamamoto S, Kawasaki T, Kohgo T, Uo M, et al. Tissue response to a newly developed calcium phosphate cement containing succinic acid and carboxymethyl-chitin. J Biomed Mater Res A 2003;64:491–501.
[36] Gu YW, Khor KA, Cheang P. Bone-like apatite layer formation on hydroxyapatite prepared by spark plasma sintering (SPS). Biomaterials 2005;25:4127–34.
[37] Koyama S, Endo M, Kim YA, Hayashi T, Yanagisawa T, Osaka K, et al. Role of systemic T-cells and histopathological aspects after subcutaneous implantation of various carbon nanotubes in mice. Carbon 2006;44:1079–92.
[38] Usui Y, Aoki K, Narita N, Murakami N, Nakamura I, Nakamura K, et al. Carbon nanotubes with high bone-tissue compatibility and bone-formation acceleration effects. Small 2008;4:240–6.
[39] Sato Y, Yokoyama A, Shibata KI, Akimoto Y, Ogino S, Nodasaka Y, et al. Influence of length on cytotoxicity of multi-walled carbon nanotubes against human acute monocytic leukemia cell line THP-1 *in vitro* and subcutaneous tissue of rats *in vivo*. Mol BioSyst 2005;1:176–82.
[40] Yokoyama A, Sato Y, Nodasaka Y, Yamamoto S, Kawasaki T, Shindoh M, et al. Biological behavior of hat-stacked carbon nanofibers in the subcutaneous tissue in rats. Nano Lett 2005;5:157–61.
[41] Carrero-Sanchez JC, Elias AL, Mancilla R, Arrellin G, Terrones H, Laclette JP, et al. Biocompatibility and toxicological studies of carbon nanotubes doped with nitrogen. Nano Lett 2006;6:1609–16.
[42] Elías AL, Carrero-Sánchez JC, Terrones H, Endo M, Laclette JP, Terrones M. Viability studies of pure carbon- and nitrogen-doped nanotubes with entamoeba histolytica: from amoebicidal to biocompatible structures. Small 2007;3:1723–9.
[43] Kostarelos K, Lacerda L, Pastorin G, Wu W, Wieckowski S, Luangsivilay J, et al. Cellular uptake of functionalized carbon nanotubes is independent of functional group and cell type. Nat Nanotechnol 2007;2:108–13.
[44] Dumortier H, Lacotte S, Pastorin G, Marega R, Wu W, Bonifazi D, et al. Functionalized carbon nanotubes are non-cytotoxic and preserve the functionality of primary immune cells. Nano Lett 2006;6:1522–8.
[45] Miyawaki J, Yudasaka M, Azami T, Kubo Y, Iijima S. Toxicity of single-walled carbon nanohorns. ACS Nano 2008;2:213–26.
[46] Eedy DJ. Carbon-fibre-induced airborne irritant contact dermatitis. Contact Dermatitis 1996;35:362–3.
[47] Shaffer MSP, Fan X, Windle AH. Dispersion and packing of carbon nanotubes. Carbon 1998;36:1603–12.
[48] Ogino S, Sato Y, Yamamoto G, Sasamori K, Kimura H, Hashida T, et al. Relation of the number of cross-links and mechanical properties of multi-walled carbon nanotube films formed by a dehydration condensation reaction. J Phys Chem B 2006;110:23159–63.
[49] Muller J, Huaux F, Fonseca A, Nagy JB, Moreau N, Delos M, et al. Structural defects play a major role in the acute lung toxicity of multiwall carbon nanotubes: toxicological aspects. Chem Res Toxicol 2008. doi:10.1021/tx800101p.
[50] Fenoglio I, Greco G, Tomatis M, Muller J, Raymundo-Pinero E, Beguin F, et al. Structural defects play a major role in the acute lung toxicity of multiwall carbon nanotubes: physicochemical aspects. Chem Res Toxicol 2008. doi:10.1021/tx800100s.
[51] Fitzer E, Heüttiner W, Claes L, Kinzl L. Torsional strength of carbon fibre reinforced composites for the application as internal bone plates. Carbon 1980;18:383–7.
[52] Baker SE, Cai W, Lasseter TL, Weidkamp KP, Hamers RJ. Covalently bonded adducts of deoxyribonucleic acid (DNA) oligonucleotides with single-wall carbon nanotubes: synthesis and hybridization. Nano Lett 2002;2:1413–7.
[53] Balavoine F, Schultz P, Richard C, Mallouh V, Ebbesen TW, Mioskowski C. Helical crystallization of proteins on carbon nanotubes: a first step towards the development of new biosensors. Angew Chem Int Ed 1999;38:1912–5.
[54] Chen RJ, Zhang Y, Wang D, Dai H. Noncovalent sidewall functionalization of single-walled carbon nanotubes for protein immobilization. J Am Chem Soc 2001;123:3838–9.
[55] Akasaka T, Watari F, Sato Y, Tohji K. Apatite formation on carbon nanotubes. Mater Sci Eng C 2006;26:675–8.
[56] Zhao B, Hu H, Mandal SK, Haddon RC. A bone mimic based on the self-assembly of hydroxyapatite on chemically functionalized single-walled carbon nanotubes. Chem Mater 2005;17:3235–41.

カーボンナノチューブの表面改質に関わる細胞毒性

Cytotoxicity concerning surface treatment of carbon nanotubes

佐藤 義倫　東北大学 大学院 環境科学研究科 環境科学専攻　助教

〒980-8579　宮城県仙台市青葉区荒巻字青葉 6-6-20，Tel 022-795-3868，Fax 022-795-3868，

E-mail：hige@bucky1.kankyo.tohoku.ac.jp

1 はじめに

悪性中皮種を発現するアスベスト[1]に形状が似ている繊維状のカーボンナノチューブ（Carbon Nanotubes: CNTs）[2]は毒性を示すのだろうか？細胞毒性を引き起こす要因には，金属溶出[3]，表面官能基[4,5]，比表面積，サイズ効果[6-9]が知られている。金属溶出は金属表面が体内の酸性により腐食し，イオンとして溶出することによって細胞に影響を与える（金属腐食）。細胞や組織内での金属腐食は最も知られた細胞毒性を引き起こす要因であり，金属のイオン化傾向に依存すると言われる。例えば，インプラント材料であるTi合金（Ti-6Al-4V）のAlはしばしば溶出し[10]，骨の成長阻害因子やアルツハイマー病の発症因子の原因として挙げられ[11]，またNiやVの溶出は強い細胞毒性を示す。Fe^{2+}は触媒作用を示し，過酸化水素からヒドロキシルラジカルや，過酸化脂質からアルコキシルラジカルを産出し，酸化性ストレスを誘導するという報告がある。さらに，磁性酸化鉄（Fe_3O_4）はアルツハイマー病，パーキンソン病などの神経退化性疾患と関連していると指摘されている[12-14]。表面官能基による毒性要因の例は，表面を覆う官能基の種類から由来する毒性である。細胞標識として注目されているCdSe量子ドットをCOOH/OHが混在した表面修飾したものは細胞毒性を示さず，COOHのみの表面修飾では細胞毒性を示すと報告されている[4]。一方，ナノ粒子の生体影響を考えるときに粒径が極めて小さくなると（サイズ依存性），ナノ粒子表面の物理的性質（高比表面積，表面電子状態の活性化），化学的性質と細胞との相互作用によるナノ粒子の体内挙動が問題となる。生体界面活性剤で被覆された金粒子は生体親和性があるが[5]，直径1.4 nmの金ナノ粒子は電子状態の変化により被覆された生体界面活性剤が外れ，DNAに吸着して安定化してしまう。この金ナノ粒子に吸着されたDNAは正常に働かず，毒性を引き起こす[9]。一般に生体親和性の高いテフロン[6]やTi[7,8]もナノサイズになると肺毒性，細胞毒性を示すことが知られている。一方，1970年代に米国のスタントン[15]と西ドイツのポット[16]は独自に繊維状形態に着目し，サイズ（長さ，直径）を調製した様々な物質をラットやマウスの胸腔，腹腔に注入し長期間飼育後，胸腔，腹腔の病変や悪性中皮種の発現率を調べている。その結果，生体内で耐久性があり，細くて長い繊維状物質は化学組成や結晶構造に関係なく発ガン性を持つことを示し，特に幅0.25 μm以下で，長さ8.0 μm以上の繊維の中皮種発現率が最も高いことを見出している。では，幾つの細胞毒性要因がCNTsに対して当てはまるのだろうか？

単層カーボンナノチューブ（single-walled carbon nanotubes；SWCNTs），多層カーボンナノチューブ（multi-walled carbon nanotubes；MWCNTs）は触媒金属を用いることにより合成される（アーク放電法で合成される多層CNTsを除く）。その触媒金属は，Fe，Co，Ni，Y，La，Ce，YNi，FeNi，CoNi，CoMo，MgO，Al_2O_3などと単体金属，合金，金属酸化物と数多く知ら

れている[17]。したがって，未精製のCNTsには金属粒子が含まれている場合がほとんどである。また，応用に応じて様々な機能性官能基を化学修飾することが可能であり，比表面積も大きい。さらに繊維状であり，直径，長さ，形態も様々である。このように，CNTsは金属溶出，表面官能基，比表面積，サイズ効果の細胞毒性を引き起こす要因を所有している。これらに加え，疎水性表面を持つCNTsは水溶液で凝集するため，凝集効果も毒性要因に加わる可能性があることも見逃してはならない。

異物が生体内に進入すると，貪食細胞（マクロファージや多核巨細胞）が異物を除去するために取り込む。その後，異物は食胞に取り囲まれ，リソソームと融合し，ファゴリソームを形成し，酵素により異物を低分子化する。低分子化された異物は無毒化され，排出される。貪食する際には，貪食細胞表面にあるレセプターにより異物を認識するが，その際にサイトカイン（種々の細胞から分泌されるホルモン様低分子蛋白の総称で，免疫反応の強さと期間を調節し細胞同士の情報交換を媒介する）を産出し，その量が毒性評価の1つになる。したがって，細胞毒性は材料と細胞との接触から誘発されるため，CNTsの表面と細胞の相互作用は重要となる。一方，医工学応用ではDNA，遺伝子の導入や形質移入のトランスポーターとしてCNTsの形状に強い関心が持たれている[18]。DNAのトランスポーターには，ウィルスベクター（レトロ，レンチ，アデノ）やカチオン脂質，ポリエチレニミン（PEI）[19]，カチオンポリマーを含む非ウィルス形質移入ベクターなどがある。これらのウィルスベクターは遺伝子の搬送を妨げる免疫反応を細胞から誘発することが多い。PEIや非ウィルス形質移入ベクターはこの問題を回避できるが，核膜浸透，遺伝子発現効率が低いことが問題となっている。いずれにせよ，トランスポーターは目的の細胞へ辿り着く前に貪食されず，かつ目的細胞へ潜り込む機能を持たせなくてはならない。CNTsのトランスポーターとして使用するには，CNTs表面への修飾を施すことになるが，施されたCNTsが毒性を示しては意味が無くなってしまう。

以上のことから，細胞とCNTs表面の接触が細胞毒性に大きく関わっているため，本稿ではCNTsの表面に関わる細胞毒性について最近の動向を報告する。

2 未化学修飾のCNTsの細胞毒性

Monteiro-Riviereら[20]，ヒト表皮細胞に対して竹の子構造を持つMWCNTs（CVD法）の影響を生体外（in vitro）試験により調べている。MWCNTsは培養液に0.1，0.2，0.4 mg/mLの濃度に調製し，ヒト由来の表皮細胞と混合し24時間培養した。MWCNTsはサイトカインであるIL-8（インターロイキン8；急性期炎症反応における好中球遊走，活性化にかかわる本質的な因子）を誘発し，細胞生存率が減少することを時間依存性，濃度依存性試験から確認している。さらに透過型電子顕微鏡（transmission electron microscope；TEM）からは，表皮細胞内にMWCNTsが存在することも観察された（図1）。つまり，MWCNTsは貪食されていたことになる。このことから，ヒト表皮細胞に対してMWCNTsは毒性を示すと考察している。

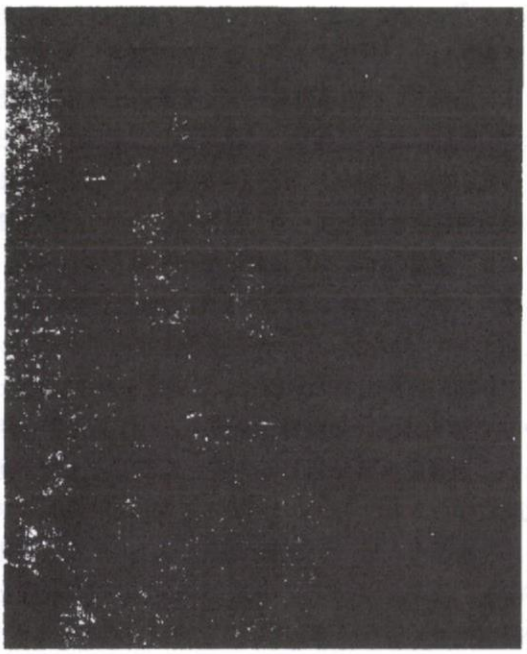

図1　表皮細胞の小胞内の透過型電子顕微鏡写真，矢印で示されている物質が竹の子状のMWCNTs[20]

Mullerら[21]，「精製MWCNTs」と「精製MWCNTsの粉砕物」を調製し，20，50，100 μg/mLの濃度を腹膜マクロファージ（マクロファージ；異物を貪食する